TAMPEREEN TEKNILLINEN YLIOPISTO
TAMPERE UNIVERSITY OF TECHNOLOGY

Jonna Kannosto

Measurement of the Physical Properties of Secondary Organic Aerosol Particles

Julkaisu 1071 • Publication 1071

Tampere 2012

Tampereen teknillinen yliopisto. Julkaisu 1071
Tampere University of Technology. Publication 1071

Jonna Kannosto

Measurement of the Physical Properties of Secondary Organic Aerosol Particles

Thesis for the degree of Doctor of Science in Technology to be presented with due permission for public examination and criticism in Sähkötalo Building, Auditorium S4, at Tampere University of Technology, on the 14th of September 2012, at 12 noon.

Tampereen teknillinen yliopisto - Tampere University of Technology
Tampere 2012

Doctoral candidate: Jonna Kannosto, M.Sc
Aerosol Physics Laboratory
Department of Physics
Tampere University of Technology
Present address:
Dekati Ltd., Tampere

Supervisors: Jorma Keskinen, prof.
Aerosol Physics Laboratory
Department of Physics
Tampere University of Technology

Annele Virtanen, assoc. prof.
Aerosol Physics Laboratory
Department of Physics
Tampere University of Technology
Present address:
Department of Applied Physics
University of Eastern Finland, Kuopio

Pre-examiners: Urmas Hõrrak, PhD
Laboratory of Environmental Physics
Institute of Physics
University of Tartu

Joakim Pagels, PhD
Ergonomics & Aerosol Technology
Department of Design Sciences
Lund University

Opponent: Heikki Lihavainen, PhD
Finnish Meteorological Institute

ISBN 978-952-15-2902-3 (printed)
ISBN 978-952-15-2980-1 (PDF)
ISSN 1459-2045

Abstract

The work of this thesis concentrates on applying the Electrical Low Pressure Impactor (ELPI, Dekati Ltd.) and scanning/differential mobility particle sizer (SMPS/DMPS) to estimate the particle density and particle solidity of secondary organic aerosols (SOA) d_{me} < 200 nm.

The density estimation method has been extended to smaller particle sizes and the data treatment of the method has been modified to be suitable for large data series and multimodal size distributions. The limitations of the method have been studied using both laboratory tests and simulations. The lowest mode particle diameter for the density method was found to be 10 nm. For multimodal size distributions, the density results varied approximately by 15 %. The density measurements were performed at the SMEAR II station and the density of boreal forest particles was measured.

The ELPI was used to study the physical phase of the fresh SOA particles formed by ozonolysis of pure α-pinene and volatile organic compounds (VOCs) of a living Scots pine in a chamber. The phase of SOA particles formed in the boreal forest was analyzed as well. The particles were found to bounce from smooth impaction plates of ELPI towards lower impactor stages. The behavior was interpreted as an indication of a solid physical phase of the particles. The interpretation was corroborated by SEM (Scanning electron microscope) images. In the TEM (Tunneling electron microscope) analysis, the particles were non-crystalline. Based on these results, the particles were inferred to have adopted an amorphous (glassy) physical state. The α-pinene particles had similar bouncing ability as the Scots pine derived particles indicating similar physical phase behavior.

The measured bounce factor did not significantly change during the particle growth for particles larger than 40 nm, indicating no changes in particle solidity. For the smallest particles (below 40 nm), the calculated bounce factor increased as the particles grew, indicating that the smallest particles were less solid than the larger ones. The maximum value of the bounce factor decreased for subsequent impactor stages of ELPI. According to a simplified model, this can be explained as a combined

effect of bounce probability and charge transfer between the particles and the impaction surface if at least 60% of the particles bounce.

The observed solidity of the SOA particles challenges the traditional views on the kinetics and thermodynamics of SOA formation, their transformation in the atmosphere and their implications on air quality and climate. It can influence the ability of the particles to accommodate water and act as could condensation nuclei or as ice nuclei, reduce the rate of heterogeneous chemical reactions and eventually alter the atmospheric lifetime of the particles.

Acknowledgements

Research for this thesis was performed in the Aerosol Physics Laboratory at Tampere University of Technology. First of all, I want to thank Professor Jorma Keskinen as the head of laboratory and Physics Department for providing the working facilities and as a supervisor for guidance and all the help. I want to thank my other supervisor, Associate Professor Annele Virtanen, for all the help and enthusiasm.

I wish to thank all the present and previous coworkers in the Aerosol Physics Laboratory. I have gotten good friends and lot of help during the time in Aerosol laboratory. Jyrki Ristimäki, Mikko Lemmetty and Heino Kuuluvainen have helped me with the density estimation method and Matlab. Jaakko Yli-Ojanperä has been helping me in the laboratory measurements. Topi Rönkkö has given me a lot of good ideas and has been a very nice roommate. Kaisa, Jaakko, Juha, Janne and Mikko, you have given me a lot of joy to my working days and conference trips.

Research is a group work and the measurements of this thesis would have not been performed without the help of people at the SMEAR II measurement station and Professor Markku Kulmala and the people at the University of Eastern Finland and Professor Jorma Joutsensaari.

I am very grateful for financial support of my research. The work is founded by the Doctoral Programme ACCC — Atmospheric Composition and Climate Change: From Molecular Processes to Global Observations and Models (funding decision number 129663) and Maj ja Tor Nessling foundation. The financial support from Henry Ford foundation, Finnish Concordia found, TES and Tamperelaisen tutkimustyön tukisäätiö is appreciated.

Lopuksi haluan kiittää vanhempiani, sisaruksiani ja ystäviäni. Kiitos, että haluatte olla osa elämääni, tätä värikästä touhua ja tohinaa. Haluan antaa erityiskiitokset Api-pappalle, joka on ollut mittaus- ja konferenssimatkojen aikana auttamassa lastenhoidossa. Erkki Koskenniemelle kuuluu valtavan suuri kiitos siitä, että kuuntelemalla ja selkeillä neuvoillasi olet antanut minulle voimaa ja oikean suunnan tehdessäni väitöskirjaa. Suurin kiitos kuuluu perheelleni. Kiitos Niklas ja Ossi, että olette antaneet päiviini loputtomasti iloa ja pieniä ihmeitä. Olette minulle valtavan tärkeitä. Viimeisenä haluan kiittää rakasta miestäni, joka jaksoi tukea ja kannustaa loppuun asti. Olet minulle kaikkeni.

List of publications

1. **PAPER I**
   J. Yli-Ojanperä, J. Kannosto, M. Marjamäki, J. Keskinen, Improving the nanoparticle resolution of the ELPI, *Aerosol and Air Quality Research,* **10**: 360–366, 2010
2. **PAPER II**
   J. Kannosto, J. Ristimäki, A. Virtanen, P. Aalto, M. Kulmala, J. Keskinen, Density analysis of boreal forest aerosols, *Chemical Engineering Transactions*, **10**, 95-99, 2006
3. **PAPER III**
   J. Kannosto, A. Virtanen, M. Lemmetty, J.M. Mäkelä, J. Keskinen, H. Junninen, T. Hussein, P. Aalto, M. Kulmala, Mode resolved density of atmospheric aerosol particle, *Atmospheric Chemistry and Physics*, **8**, 5327-5337, 2008
4. **PAPER IV**
   A.Virtanen, J. Joutsensaari, T. Koop, J. Kannosto, P. Yli-Pirilä, J. Leskinen, J. Mäkelä, J. Holopainen, U. Pöschl, M. Kulmala, D. Worsnop, A. Laaksonen, An amorphous solid state of biogenic secondary organic aerosol particles, *Nature,* **467**, 824-827, 2010
5. **PAPER V**
   A.Virtanen, J. Kannosto, J. Joutsensaari, E. Saukko, H. Kuuluvainen, L. Hao, P. Yli-Pirilä, P. Tiitta, J. K. Holopainen, D. R. Worsnop, J. N. Smith, A. Laaksonen, Bounce behavior of freshly nucleated biogenic secondary organic aerosol particles, *Atmospheric Chemistry and Physics*, **11**, 8759-8766, 2011
6. **PAPER VI**
   J. Kannosto, P. Yli-Pirilä, L. Hao, J. Mäkelä, J. Joutsensaari, A. Laaksonen, D. R. Worsnop, J. Keskinen, A. Virtanen, Bounce characteristics of α-pinene derived SOA particles with implications to physical phase, Accepted *Boreal Environment Research*, 2012

Author's contributions

1. **PAPER I**
   J. Yli-Ojanperä, J. Kannosto, M. Marjamäki, J. Keskinen, Improving the nanoparticle resolution of the ELPI, *Aerosol and Air Quality Research,* **10**: 360–366, 2010
   - I performed all the density measurements and the simulations. Further, I performed the required development of the density analyzing method and the data processing of the density analysis. I also had the main responsibility in writing the density analyzing part.

2. **PAPER II**
   J. Kannosto, J. Ristimäki, A. Virtanen, P. Aalto, M. Kulmala, J. Keskinen, Density analysis of boreal forest aerosols, *Chemical Engineering Transactions*, **10**, 95-99, 2006
   - I performed most of the density measurements and all the data processing and most of the required development of the density analyzing method. Also, I had the main responsibility in the writing process.

3. **PAPER III**
   J. Kannosto, A. Virtanen, M. Lemmetty, J.M. Mäkelä, J. Keskinen, H. Junninen, T. Hussein, P. Aalto, M. Kulmala, Mode resolved density of atmospheric aerosol particle, *Atmospheric Chemistry and Physics*, **8**, 5327-5337, 2008

   - I performed most of the density measurements, part of the sensitivity simulations and all the data processing. In addition, I performed most of the required development of the density analyzing method and had the main responsibility in the writing process.

4. **PAPER IV**
   A.Virtanen, J. Joutsensaari, T. Koop, J. Kannosto, P. Yli-Pirilä, J. Leskinen, J. Mäkelä, J. Holopainen, U. Pöschl, M. Kulmala, D. Worsnop, A. Laaksonen, An amorphous solid state of biogenic secondary organic aerosol particles, *Nature,* **467**, 824-827, 2010

   - I participated in the particle measurements in the chamber, in boreal forest and in the laboratory. I also performed most of the ELPI data analysis and took part in the writing process.

5. PAPER V

A.Virtanen, J. Kannosto, J. Joutsensaari, E. Saukko, H. Kuuluvainen, L. Hao, P. Yli-Pirilä, P. Tiitta, J. K. Holopainen, D. R. Worsnop, J. N. Smith, A. Laaksonen, Bounce behavior of freshly nucleated biogenic secondary organic aerosol particles, *Atmospheric Chemistry and Physics*, **11**, 8759-8766, 2011

- I performed a part of ELPI measurements in the chamber and participated in the ELPI data analysis. I also had a minor responsibility in the writing process.

6. PAPER VI

J. Kannosto, P. Yli-Pirilä, L. Hao, J. Mäkelä, J. Joutsensaari, A. Laaksonen, D. R. Worsnop, J. Keskinen, A. Virtanen, Bounce characteristics of α-pinene derived SOA particles with implications to physical phase, Accepted *Boreal Environment Research*, 2012

- I performed a part of the particle measurements and all the data analysis. I had the main responsibility in the writing process.

Nomenclature

AMS	Aerosol Mass Spectrometer
FEP	Fluorinated ethylene propylene
CFD	Computational Fluid Dynamics
CPC	Condensation Particle Sizer
DMA	Differential Mobility Analyzer
DMPS	Differential Mobility Particle Sizer
DOS	Di-octyl-sebacate
ELPI	Electrical Low Pressure Impactor
GMD	Geometric Mean Diameter
GSD	Geometric Standard Deviation
PS	Polystyrene
RH	Relative Humidity
SEM	Scanning Electron Microscope
SMPS	Scanning mobility particle sizer
SOA	Secondary Organic Aerosol
STD	Standard Deviation
TEM	Tunneling Electron Microscopy
VOC	Volatile Organic Species

AP_n	Apparent bounce probability in stage n
BF_n	Bounce factor in stage n
C_c	Cunningham correction factor
d_a	Aerodynamic diameter
d_{me}	Mobility diameter
d_m	Mass equivalent diameter
E_{ch}	Charger efficiency function
I	Current
k_j	Kernel function
n	Number concentration
P_n	True bounce
q_T	Transferred charge
q_C	Contact charge
q_0	Precharge
q_n	Charge leaved to the stage n by a single particle

Z	Space-charging
β	Fraction of precharge transferred
ρ_e	Effective density
ρ_0	Unit density
ρ_p	Particle density
χ	Shape factor

Contents

1. Introduction

1.1. Atmospheric SOA particles

Atmospheric aerosol is complex mixture of primary and secondary particles and gas (e.g. Seinfeld and Pandis, 1998). Primary particles are directly emitted from their source, that is for example domestic combustion, road traffic, industrial activity, a volcanic eruption. The composition of primary particles varies along with their source. Secondary particles, on the other hand, are formed in the atmosphere by gas-to-particle conversion processes such as nucleation and condensation. In the atmosphere, the secondary aerosol (SOA) particles consist of ammonium, sulfates and a wide variety of organic species. The composition and number of the SOA particles changes along with the source of organic matter which can be, for example a boreal forest, an ocean or domestic heating or cooking (Hallquist et al. 2009, Kulmala et al. 2011). The chances in composition also affect the physical properties of particles. Particle size and composition affect the particle residence time in the atmosphere, the potential of particles to act as cloud condensation nuclei, their optical properties and behavior and their deposition in human lungs. SOA particles are very significant in the atmosphere (Hallquist et al. 2009, Kanakidou et al. 2005). It has been estimated that 60 % – 70 % of the total organic aerosol mass is SOA in the global scale and that the formation of SOA can be as significant as emission of POA (primary organic aerosol) (Hallquist et al. 2009, Kanakidou et al. 2005). SOA particles affect the radiation balance and climate of the Earth by scattering radiation, acting as cloud condensation nuclei and they participate in the formation of ice nuclei. Particles also affect air pollution and quality and, therefore human health and they have been linked to untimely deaths. They can also decrease visibility of atmosphere. Therefore, it is important to understand the properties of particles and, especially, to provides tools for modeling the weather and climate change and minimizing the negative health effects.

The properties of the smallest atmospheric particles are not very well known and, also, their formation processes are partly unknown. The composition and the properties of accumulation mode ($d_{me} > 100$ nm) particles are fairly well understood as proper measurement techniques are available in this size range and the mass concentration level is adequate for analyzes (e.g. Wall et al. 1988, Maenhaut et al.

1999, Putaud et al. 2004, Cross et al. 2007, Hu et al. 2011, Slowik et al. 2004). In the past few years, ultrafine particles (d_{me} < 100 nm) have been studied very actively, but there are still gaps in the overall knowledge about the properties, formation and chemical composition of ultrafine particles (Kulmala et al. 2004, Yu et al. 2012). Few studies in district locations have done to define the particle chemical composition for example in boreal forest (Mäkelä et al. 2001, Ebben et al. 2011). Particle density provides information regarding particle composition. For example the density of water is 1 g/cm^3 but combustion particles can have very high density values (about 2.6 g/cm^3 (SiO_2) and even higher) due to ash and metallic compounds. Organic materials on the other hand can have density values such as 0.85 g/cm^3 (α-pinene, CRC) or 0.68 g/cm^3 (dimethyl amine, CRC). The particle density measurements have been performed in urban sites (e.g. Virtanen et al. 2006, Mc Murry et al. 2002) and in boreal forests (e.g. Saarikoski et al. 2005, Paper II, Paper III). Also, studies with particle mass spectrometers provide some insight to the chemical composition of ultrafine particles (e.g. Smith et al. 2005, Huang et al. 2010).

Gas-to-particle models usually assume that SOA particles are liquid (Marcolli et al. 2004, Pankow 1994, Odum et al. 1996). However, recent experiments have shown that atmospheric SOA particles can also be glassy (solid) (Paper IV, Paper V, Paper VI). This new finding has an influence on understanding of the particle properties such as water uptake or atmospheric processes as cloud condensation (Paper IV).

In this thesis, an electrical low pressure impactor (ELPI, Dekati Ltd.) was used to measure density and solidity of particles. The density analysis is based on the parallel measurement of an ELPI and a SMPS/DMPS. The method calculates effective density for particles larger than 10 nm (Paper I, Paper II, Paper III). In action, the method can measure the density as a function of time. The density analysis method was applied in rural environment (Virtanen et al. 2006) and in the study of boreal forest SOA particles (Paper II, Paper III). The effective density value was able to detect for nucleation, Aitken and accumulation modes as a function of time (Paper III). The density of the nucleation mode particles was able to measure during new particle events (Paper III).

The physical state of ultrafine particles can also be studied solely with ELPI measurements. Liquid particles stick on ELPI impactor plates, whereas glassy (solid) and crystalline (solid) particles can bounce from the impactor plates. The particle bounce can be detected in ELPI measurements and, thus, the instrument can be used

as a solidity indicator. The amount of bounce as well as the changes in the bouncing characteristics of the particles can be calculated from ELPI currents. An ELPI was used to study the solidity of α-pinene derived SOA particles, boreal forest SOA particles and particles produced by VOC (volatile organic compounds) which were emitted from a living Scotch pine. Changes in the bounce ability of particles were studied during growth processes. (Paper IV, Paper V, Paper VI).

1.2. ELPI Instrument

To understand the method presented in this thesis, the operation principle of the ELPI (Electrical Low Pressure Impactor, Dekati Ltd.) needs to be understood. An ELPI is an instrument based on charging the particles with a diffusion charger, passing them through a cascade impactor and measuring the electrical current caused by charged particles at each impactor stage. The instrument measures concentration as a function of aerodynamic size of particles in real time. The ELPI was developed in Aerosol physic laboratory of Tampere University of Technology (Keskinen et al. 1992) and nowadays it is widely used for various applications in several countries. This thesis is based on ELPI measurements and mathematical modeling of the instrument.

Construction and operating principle

In the ELPI instrument, the sample aerosol is first led through a diffusion charger. The charger is a cylinder having a high voltage corona needle electrode placed in its center. The corona needle generates positive ions which travel towards the cylinder wall due to the produced electric field. The aerosol particles pass through the positive ion plume and become charged by the ions. The charging process is mainly governed by diffusion of ions onto particle surface. The charge level of the particles is a function of particle mobility diameter (d_{me}) (Marjamäki et al., 2000).

After the charger, the charged aerosol particles are led to a cascade impactor where the particles are size classified. The cascade impactor consists of 12 impactor stages in series. Inside an impactor stage, the aerosol is led through small nozzles and, in consequence of this, it will accelerate. After passing the nozzles, the gas makes a sharp turn in front of a collection plate. Particles larger than a critical size, which is

specific for each impactor stage, are not able to follow the gas stream because of their inertia but, instead they impact onto the collection plate. Conversely, particles smaller than the critical size do not impact but follow the gas stream to the next impactor stage. The stages further down the cascade impactor have smaller critical sizes. The impaction depends on particle geometric size, shape, and density. These factors are usually incorporated into a single quantity called the aerodynamic diameter of particles (d_a).

Particles having small aerodynamic size can follow the gas stream longer than those having larger aerodynamic size. The classic version of the ELPI impactor covers the aerodynamic size range of 28 nm – 6.6 µm. When small particles are present, filter stage can be inserted under the lowest stage. The filter stage collects particles smaller than the critical of the lowest impactor stage (Marjamäki et al., 2002). Thus, the size range of the ELPI impactor is 7 nm – 6.6 µm. In this thesis, the filter stage was used in all measurements.

The impaction of charged particles onto the impactor plates can be detected as a current. The current of each stage is measured using very sensitive electrometers. The maximum time resolution of the instrument is in the order of one second, but the noise level of the electrometers increases with frequency bandwidth. With an averaging time of 60 s, which is typical to low concentration measurements, the detection level of current is approximately 1 fA. The measured current signals are detected and saved whith an external computer using the ELPI measurement program. The concentration of particles can be calculated from the amount of current detected at each stage. In this thesis, the ELPI currents have not been converted to particle concentrations. The flow that carries the aerosol through the charger and the impactor is generated with a vacuum pump. The flow is controlled using an external valve located after the ELPI unit. The nominal flow of the classic ELPI and Outdoor ELPI are 10 Lpm and 40 Lpm , respectively.

Instrument Calibration and Mathematical Modeling

Charger calibration can be performed with a particle generator, neutralizer + charger and a Faraday Cup Electrometer (FCE) in series. The current of the charged particles which are deposited on the filter in the FCE is measured with and without the charger. This measurement is performed with different particle mobility diameters

(d_{me}) to gain the response of the particles. This is defined as "penetration" ($Pn(d_{me})$). The procedure is described in detail in Marjamäki et al. (2000). For this study, the primary result of the calibration is the particle mobility diameter dependent charger efficiency function $E_{ch}(d_{me})$. The following fitted functions are used to calculate numerical values for $E_{ch}(d_{me})$.

$$E_{ch}(d_{me}) = Pn(d_{me})eQ, \quad (1.1)$$

where $Pn(d_{me})$ is the penetration of particles having mobility diameter d_{me} through the charger (gained by charger calibration), Q is aerosol flow and e is the elementary charge.

$$Pn(d_{me}) = 222.49 d_{me}^{1.637}, d_{me} \leq 0.023\mu m \quad (1.2)$$

$$Pn(d_{me}) = 68.12 d_{me}^{1.32}, d_{me} > 0.023\mu m$$

The current $i(d_{me})$ that is carried into the impactor by concentration $n(d_{me})$ of particles having mobility diameter d_{me} is then given by:

$$i(d_{me}) = E_{ch}(d_{me})n(d_{me}) \quad (1.3)$$

The impactor calibration means that the kernel functions of the stages of the cascade impactor are measured. The kernel function $k_j(d_a, d_{me})$, of the stage *j* is the fraction of the particles entering the cascade impactor that get collected at the stage *j*. The primary collection (impaction) of the particles depends on their aerodynamic diameter (d_a) that is function of mobility diameter (d_{me}) and particle density (Eq. 2.1). In addition to impaction, particles are deposited by diffusion and Coulombic interaction, depending on their mobility diameter (Virtanen et al., 2001). Here, the secondary collection of particles through the space charge effect is neglected as the concentrations are too low for that in atmospheric aerosol measurements.

In the laboratory calibration, particles are produced from DOS (di-octyl-sebacate, density ρ_e=0.91 g/cm^3) using an evaporation - condensation generator. After the generation, DMA (differential mobility analyzer) is used to separate particles having of a chosen mobility diameter. The electrical current response of ELPI for the single size particles is measured and after measurement the particle size is changed. The response measurement is repeated until the whole range of the ELPI impactor has been covered. The calibration procedure is described in Keskinen et al. 1999.

Combining the charger efficiency function and the impactor kernel functions, the current of the impactor stage (or instrument channel) *j* can be calculated with the following equation

$$I_j = \int_0^\infty k_j(d_a, d_{me}) i(d_{me}) \mathrm{d}d_{me} = \int_0^\infty k_j(d_a, d_{me}) E_{ch}(d_{bme}) n(d_{me}) \mathrm{d}d_{me} \quad (1.4)$$

where the integration is over the mobility diameter range of the measured aerosol size distribution. Note that for each mobility diameter also the aerodynamic diameter needs to be known.

2. Particle density measurement

Particle aerodynamic diameter and mobility diameter are related through the effective density (ρ_e) of the particles (Ristimäki et al., 2002):

$$d_a{}^2 C_c(d_a) \rho_0 = d_{me}{}^2 C_c(d_{me}) \rho_e \,, \quad (2.1)$$

where ρ_0 is unit density and C_c is Cunningham slip correction factor. The effective density of the particle is dependent on particle material density, porosity and shape. For spherical non-porous particles, the effective density equals the material density. As the aerodynamic diameter can now be written as a function of mobility diameter and effective density, the current of the ELPI channel *j* can be written as follows:

$$I_j = \int_0^\infty k_j(\rho_e, d_{me}) E_{ch}(d_{me}) n(d_{me}) \mathrm{d}d_{me} \quad (2.2)$$

The particle mobility size distribution can be measured with a scanning mobility particle sizer (SMPS) and the particle aerodynamic size distribution can be measured with an ELPI.

Next, the procedure to define effective density is introduced. First, a mode is fitted to the measured SMPS size distribution. The fitted mode is multiplied with the charger efficiency ($E_{ch}(d_{me})$) and then integrated with the kernel functions $k_j(\rho_e, d_{me})$ using an assumed value for effective density. The result is simulated currents (I_j), see Eq. 2.2. The closer the assumed density value is to the real one, the better is the match between the simulated and the measured currents. Therefore, the effective density of particles can be estimated by minimizing the difference between the simulated and

the measured currents. The minimization is performed by altering the effective density in the current simulation procedure. This method is schematically described in Figure 2.1.

This density estimation method was developed at Tampere University of Technology and it was first described by Ristimäki et al. (2002). The method was first applied to laboratory aerosols and diesel exhaust particles and then developed further to be suitable for multi-modal size distributions (Virtanen et al. 2006).

Density measurement for atmospheric aerosols

The data treatment of the method has been modified to be suitable for large data series of multimodal size distributions, which is typical for atmospheric aerosols. In most cases, the shapes of aerosol distributions are relatively close to lognormal distributions. Thus, the measured number size distribution is divided into lognormal sub-distributions (modes). The automatic algorithm described by Hussein et al. (2005) is used to fit 1 to 3 lognormal distributions of the size distributions measured by differential mobility particle sizer (DMPS). The main difference to the single mode case (Ristimäki et al. 2002) is that, instead of one effective density, the effective density for each mode is searched. This means that the search algorithm has to operate in multi-dimensional space and the result may be more sensitive to the starting point of the search than in the single mode case. Several methods can be used to define the starting point for the search algorithm. In density estimation method, the effective densities are initialized with an *ad hoc* method where the initial effective densities are given in a sequence. The initialization starts from the distribution which contributes most to the ELPI current and ends with the one that contributes least. These contributions can be easily calculated as the total current produced by the distribution does not depend on the effective density. The actual initialization of each mode is performed by utilizing a set of pre-selected densities ranging from 0.1 to 10 g/cm^3, and then choosing the density which gives the smallest difference between the measured and the simulated currents. After the initialization, the search algorithm (achieved with the “fminsearch“ function of Matlab®) minimizes the difference between the measured and the simulated ELPI currents by altering the effective density of each mode.

1. Modes are fitted to data measured by DMPS representing nucleation, Aitken and accumulation mode

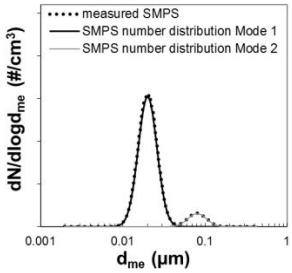

2. Modes are multiplied with the charger efficiency ($E_{ch}(d_{me})$)

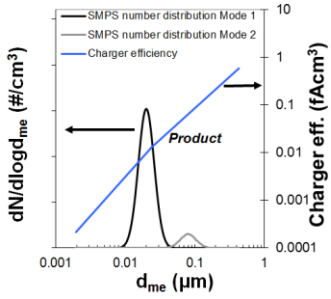

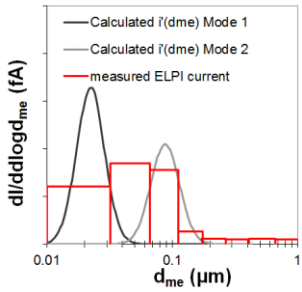

and the result is calculated "electric current modes"

3. Current modes are integrated with kernel functions

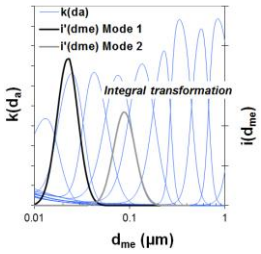

Minimizing the difference between measured and simulated ELPI currents by altering the effective density of each mode

4. Result is simulated ELPI currents

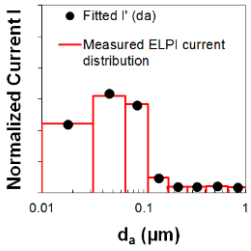

5. Result is the effective density (ρ_e) of each mode

Figure 2.1 The diagram of particle density calculation

2.1. Limitations of density measurements

The focus of aerosol studies has moved toward ever smaller particles during the last years. To gain better size resolution and to improve the density estimation for nucleation particles, a new impactor state was developed. The new impactor stage was developed to complement the classic impactor and add resolution for small particles. The new stage was inserted between the first stage and the filter stage. In the impactor, the filter is in the bottom and then the stage having lowest cut-point. The lowest cut-point of the classic impactor is 32 nm whereas the cut-point of the new impactor stage is 17 nm (Table 2.1). The filter stage cut-point (7 nm) is set by the charger penetration and charging efficiency and is on mobility diameter. The new stage was developed holding the classic impactor parameters, pressures and flow unchanged. One upper stage has to be removed to get physical space for the new stage. The pressure before the first stage is 100 mbar but before the new stage it is 43 mbar. The lower pressure requires a new, more effective vacuum pump, but no other changes are necessary (Paper I).

The sensitivity and reliability of the density analyzing method have been both tested in the laboratory and simulated using the new and the classic impactor setups (Paper I). The laboratory measurements show that the method works well and that the results agree well with the used bulk densities of the generated particles. However, there are many variables affecting the sensitivity of the method and the laboratory measurements are not effective enough to study all the restrictions. Therefore, a number of simulation tests were performed to determine the operation limits of the method.

Table 2.1 Cut-point (D50) values of the ELPI impactor stages, indicating the diameter of 50% collection efficiencies. Mobility diameter value for stage 0, aerodynamic diameter values for stages 1-14. (PAPER I)

	stage #	D50 (μm)
filter stage	0	0.007
new stage	1	0.017
	2	0.032
	3	0.055
	4	0.094
	5	0.157
	6	0.265
	7	0.386
	8	0.619
	9	0.956
	10	1.61
	11	2.41
	12	4.03
	13	6.74
	14	9.99

Lowest particle size for density estimation

The density estimation method was tested in the laboratory to find the lowest mode diameter limit. Single-mode size distributions of di-octyl sebacate (DOS, density 0.912 g/cm^3) aerosol were generated with an atomizer and a condensation-evaporation generator. The mode size was varied between 8 nm – 40 nm and distributions were rather narrow (standard deviation, STD, 1.2 – 1.4). The particle measurements were performed with a SMPS and an ELPI. The new impactor setup was used and the impactor collection plates were coated with greased smooth foils. The currents of the classic ELPI impactor setup were calculated by summing up the currents of the new stage and the filter stage. The density results calculated from the new and the calculated classic impactor configurations are presented in Figure 2.2. For particles larger than 15 nm, the results obtained with both impactor setups are very close to the bulk density of DOS. The deviation of the density values start to increase for particles smaller than 15 nm. The estimated density values were within

20% of the material bulk density down to 13 nm for the classic setup and down to 8 nm with the new setup.

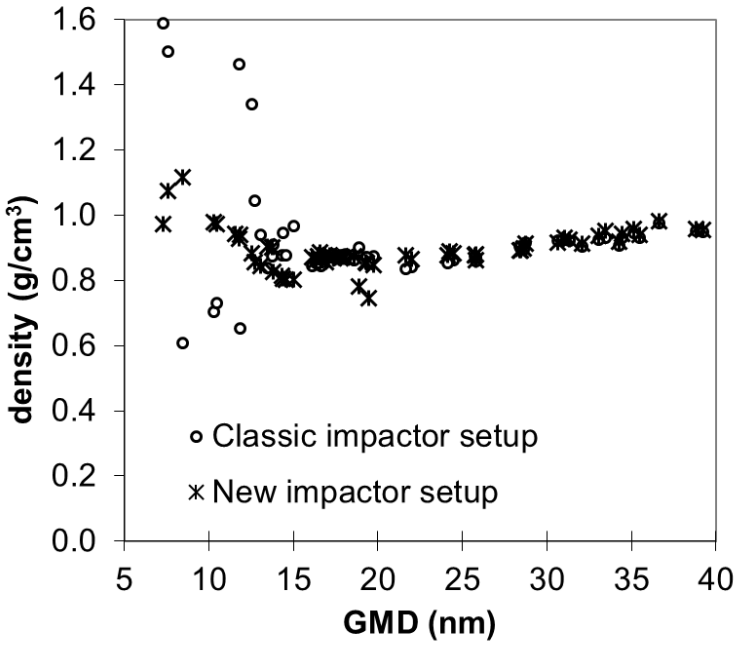

Figure 2.2. Measured density values of DOS with both new (stars) and classic (open circles) impactor setups as a function of mode geometric mean diameter (GMD) (d_{me}). (Paper I)

The simulations were performed with both the new and the classic ELPI impactor setup. A narrow single lognormal size distribution (GSD 1.2) was used and the GMD (geometrical mode diameter) changed between 6 nm – 20 nm (1 nm steps) and 20 nm – 40 nm (5 nm steps). The assumed density was 1 g/cm^3. The initial size distribution and the mathematical model of the ELPI were used to obtain the simulated currents for all stages. To test the sensitivity of the density estimation method to experimental errors, 5 % random noise was added to each simulated stage current before the density was calculated. This was repeated 50 times for each size distribution.

The output of the reliability simulation is the standard deviation (STD) of density as a result of the 50 calculations. The simulation was performed with both the new and classic ELPI impactor setups (Fig 2.3). For size distributions larger than 20 nm, the calculated density value was very close to the initial density value in both the new and the classic ELPI setups. For the classic ELPI setup, STD increases rapidly when GMD decreases below 20 nm. The scattering of the density results analyzed with the new ELPI setup is insignificant down to mode size 10 nm. The lowest GMDs producing reliable density estimates were 10 nm and 20 nm for the new and the classic impactors, respectively. These are aerodynamic diameters. The corresponding mobility diameters depend on particle density: diameters are lower if density is higher than 1 g/cm^3 and higher if the density is lower than 1 g/cm^3.

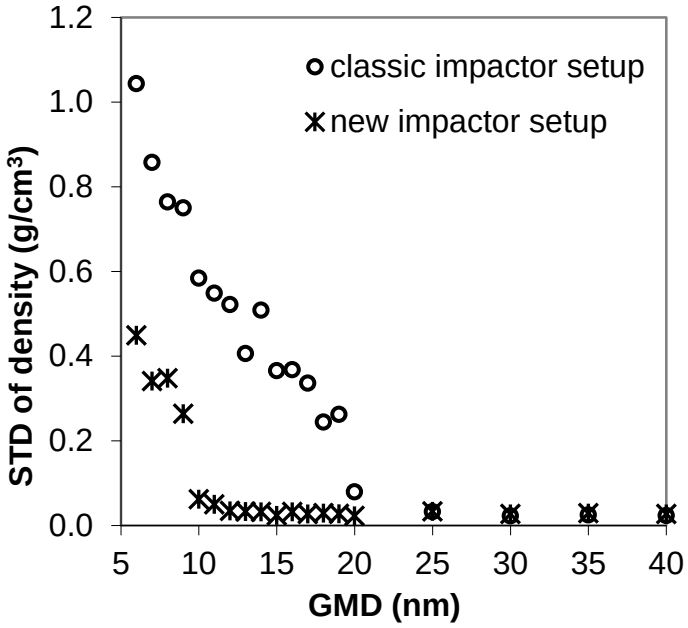

Figure 2.3. Result of the reliability simulation. STD of the analyzed densities results increases as the mode GMD decreases. The deviations of the classic impactor (open circles) and the new impactor (black stars) start to increase below 20 nm and 10 nm, respectively. (Paper I)

Operation with multimodal size distributions

Laboratory tests were conducted with bimodal distributions where one mode was composed of DOS particles and the other of Fomblin (perfluorinated polyether inert fluid, Ausimont Ltd, density 1.9 g/cm^3) particles. The Fomblin particles were generated with a tube furnace and the DOS particles with an atomizer and a condensation-evaporation generator. The GMDs of the DOS distributions varied between 40 nm – 50 nm and the GMD of the Fomblin distributions between 90 nm – 150 nm. The mobility size distribution was measured with SMPS and the aerodynamic size distribution with an ELPI. In the ELPI, the classic impactor configuration with the filter stage was used and the impactor plates were smooth and greased foils. The results obtained by the density analyzing method were 0.8 ± 0.08 g/cm^3 for DOS and 1.8 ± 0.26 g/cm^3 for Fomblin. The results varied approximately 15 % compared to the bulk density. An example of a measured bimodal size distribution and fitted lognormal modes are presented in Figure 2.4.

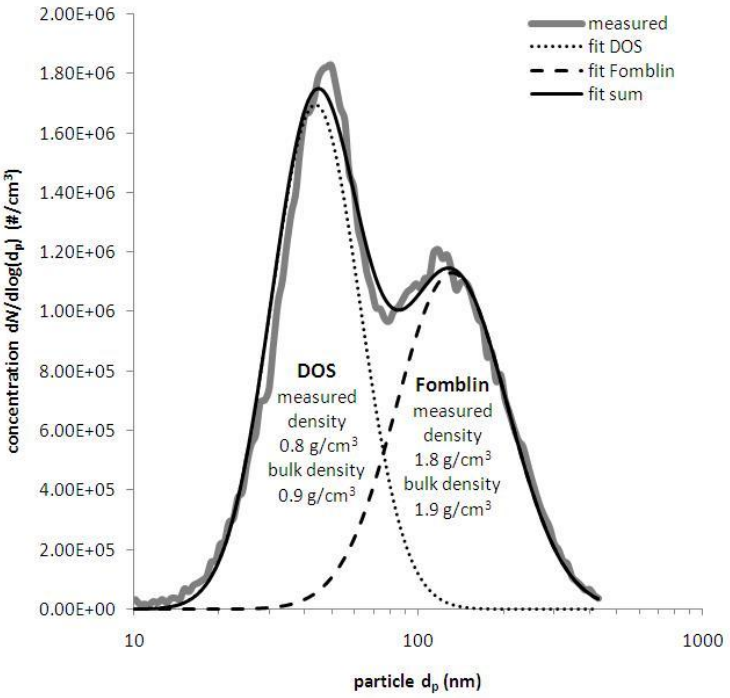

Figure 2.4. Measured bimodal size distribution consisting of DOS and Fomblin modes (fitted) and the analyzed density values of both modes.

The appliance of the method in the case of atmospheric aerosol was studied using three simulated modes to represent nucleation, Aitken and accumulation modes. The densities of the particles in the modes were varied from 0.5 g/cm^3 – 2.0 g/cm^3 and the simulated ELPI currents were calculated. Random noise (5 %) was added to the simulated all ELPI current channels and the simulated DMPS size distributions. After that, the simulated currents and DMPS distributions were used as input for the density estimation method. The density results show that reliable operation of the method mainly depends on mode size (GMD) and on the relative concentrations of the modes. The lowest mode diameter for the multimodal case to function is 15 nm – 20 nm but the circumstances must be favorable. Accurate mode fitting is important to obtain reliable mode GMD and, thus, sufficient particle concentration is required. The density value of a mode can be found if the mode produces at least approximately 20 % of the measured total current. Table 2.2 shows the required number concentrations and the minimum currents. The minimum for the nucleation mode number concentration is much larger than for the accumulation mode due to the lower charging efficiency for smaller particles. The minimum total current, 50 fA, is very small but still clearly distinguishable from the zero level of the electrometers if zeroing is done properly.

Table 2.2. The minimum concentration and currents required in the density analyzing method. (Paper III)

Minimum total current	Minimum current produced by one mode (20 %)	Corresponding concentration: nucleation mode GMD 20 nm	Corresponding concentration: accumulation mode GMD 200 nm
50 fA	10 fA	10 400 #/cm^3	240 #/cm^3

According to simulations, there is a case where the method can fail even though the minimum values are fulfilled. If two modes produce approximately the same amount of current, the two modes may swap places on the aerodynamic axis. This mode swapping can be recognized as one of the modes obtains a too large density value for

outdoor particles (> 7 g/cm^3) and the other mode obtains an improbably small value (< 0.2 g/cm^3). The possible mode swapping can be tested by calculating the aerodynamic sizes of the modes using the mobility sizes and found density values of the modes. If the modes swap places, the density results of both modes are removed from further analyses.

A third type of reliability test that was performed was a sensitivity analysis for the density values calculated from measured data. A 5 % random noise component was added to the measured ELPI currents before running the density estimation algorithm. This was repeated 100 times for each of the analyzed distributions. This procedure produces the standard deviation for each density result. The analysis is very time-consuming due to the large number of calculation runs and data points and, therefore, it can be performed only for selected occasions. This sensitivity study can be used as a tool whereby uncertain results can be removed from the further analysis. In the case of multimodal size distribution, the density results of the modes are removed differently, depending on the amount of current the mode produces. The mode is treated as the dominant mode if the mode produces most of the measured currents. In other cases, the mode is treated as a less dominant mode. If less dominant mode receives high standard deviation, only the density results of the less dominant mode are removed. If the dominant mode receives high standard deviation, the density results of all the modes of the size distribution are removed. If the added noise component causes the mode swapping, all the modes are removed. This sort of sensitivity study has been used in the results in Chapter 2.2. The results can be seen in Figure 2.8c - d.

2.2. Density measurements of boreal forest aerosol particles

Density measurements were performed at the boreal forest measurement station SMEAR II in Hyytiälä, Southern Finland (Kulmala et al. 2001). Around the measurement station, there are extensive areas of boreal forest dominated by Scots pine. The particle number concentrations are on typical rural levels (1 000 #/cm^3 – 4 000 #/cm^3, Hari and Kulmala 2009). The experiments were performed during 2 May 2005 – 19 May 2005.

Particle size distributions were measured with an ELPI (Dekati Ltd.), an Outdoor ELPI (Dekati Ltd.), a SMPS (TSI, a scanning mobility particle sizer, CPC 3025, DMA 3071) and a twin-DMPS (a differential mobility particle sizer) system (two Vienna type DMAs, with 11 cm and 28 cm tube lengths, CPC 3025, CPC 3010 (Mäkelä et al. 1997)). The measurement range both of the ELPI and the Outdoor ELPI was 7 nm – 6 µm, both were equipped with the filter stage and their flow rates were 10 lpm and 30 lpm, respectively. The averaging time for these ELPI measurements was one minute. The measurement range of the SMPS was 10 nm – 400 nm and the scanning time was 10 minutes. The DMPS size range was 3 nm – 500 nm and the scanning time was also 10 minutes. The measurement instruments were installed into two cabins and the cabins were located at 70 m distance from each other. The Outdoor ELPI and the DMPS were in one cottage and the ELPI and the SMPS in the other.

The density of nucleation, Aitken and accumulation mode particles

In this chapter, the GMDs (mobility diameters) of different modes are as follows: 15 nm – 30 nm for the nucleation mode, 30 nm – 70 nm for the Aitken mode and larger than 70 nm for the accumulation mode. The size range of the Aitken mode is chosen differently than usually (30 nm – 100 nm). This is based on the clear difference in the density values of the Aitken and the accumulation modes (see, Figures 2.5).

The density values of all modes are dispersed into two different groups. The dividing line of the two groups is approximately at 70 nm (Figure 2.5). The different density values of the Aitken and the accumulation modes indicate that the modes have different origin and, thus, 70 nm appears to be a reasonable boundary between the Aitken and the accumulation modes. The origin of the accumulation mode particles is often long-range transportation due to the inefficient particle removal mechanism in this size range (Seinfeld and Pandis 1998). The nucleation and Aitken mode particles are often formed locally, and the nucleation mode particles grow eventually to the Aitken mode sizes. Also the Aitken mode particles grow eventually to accumulation mode sizes but it takes a longer time. The density of the particles can be used to distinguish and divide the particles into the Aitken and the accumulation modes. There are no clear density differences between the nucleation and the Aitken mode but instead density decreases smoothly when particle size increases which supports the assumption that the nucleation mode particles become the Aitken mode particles by particle growth. The average value of the density results can be calculated for

particle ranges mention above and result for the nucleation mode is 1.1 g/cm^3, for the Aitken mode 0.8 g/cm^3 and for the accumulation mode 1.5 g/cm^3. These values are calculated from hour average values of currents and DMPS particle number size distribution.

The size distribution was measured with four separate instruments, although, to be able to analyze the density of the modes, only one pair of instruments based on mobility and aerodynamic separation is required. The density result was calculated using three different instrument pairs to compare the results. Thus, three density results were found for each mode. Hourly averages of the measured mobility size distributions and the measured currents were used to calculate the density values of the modes. The density results of a two week measurement campaign are presented in Figure 2.5. The average density values in 7 different size bins are shown in the figure to facilitate the comparison between the instrument pairs. The results of the Outdoor ELPI – DMPS (black dots), the ELPI – DMPS (gray dots) and the ELPI – SMPS (white dots) pairs are in good agreement. Also the standard deviation of the density results from the ELPI – DMPS is calculated and the STDs of the densities are presented as error bars in gray dots. The maximum difference of results is 17 % between instrument pairs. Thus, the density analyzing method can be applied to different instruments if the instruments are carefully calibrated, as the case was here. The STD is a result of normal random noise of the measurements but also of the diurnal variation of the densities of the modes. Therefore, the STD values for the densities are not measures of the reliability of the result.

In Figure 2.5, the average results are also compared to the results of Saarikoski et al. (2005) (grey square). Saarikoski et al. (2005) studied chemical composition of particles using a low pressure impactor in Hyytiälä. The density results were obtained from a mass closure analysis. The comparison of the density values between the density analyzing method applied here and the mass closure analysis in Hyytiälä is very good for the overlapping size range.

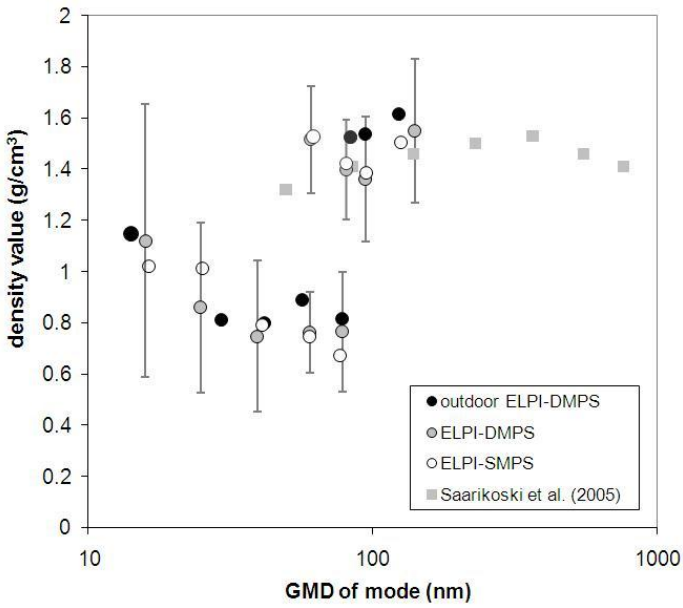

Figure 2.5. Density results as a function of mode GMD calculated from three different instrument pairs and compared with results of Saarikoski et al (2005). The results of an Outdoor ELPI – DMPS (black dots), an ELPI – DMPS (gray dots) and an ELPI – SMPS (white dots) and result of Saarikoski et al. (2005) (gray square) are presented. (Paper II)

Density variations within the campaign

The density values can also be studied as a function of time when real-time instruments are used. In Figure 2.6, the density values of nucleation (black dot), Aitken (gray triangle) and accumulation (black stars) modes are presented during the measurement campaign. The density values are calculated from 10 minutes averages of currents and DMPS number size distributions. Between the evening 16 May 2005 and the morning 18 May 2005, the instruments were not in use and, therefore, there are non data points in that time interval. The density values of the Aitken and the accumulation modes have a clearly increasing trend as a function of time. The density values of the Aitken mode and accumulation mode varied between 0.4 g/cm^3 – 2 g/cm^3 and 1.1 g/cm^3 – 2 g/cm^3, respectively. The average of the densities was 0.97 g/cm^3 and 1.5 g/cm^3 for the Aitken and the accumulation mode, respectively. The average density value for the accumulation mode agreed well with studies reported by Mc Murry et al. 2002, Paper II, Saarikoski et al. 2005 and Cozic et al. 2008.

For the nucleation and the Aitken mode, the density measurements presented in this thesis (Paper II, Paper III) were the first ones for boreal forest aerosol.

Generally, the measurement campaign can be divided into two different periods: the "No event"-period (4 – 10 May 2005) which is period without new particle formation events and the "Event"-period (11 – 20 May 2005). The lowest density values for the Aitken and the accumulation modes occur in the beginning of the measurement campaign. The density value for the accumulation mode increases during the "No event"-period and reached the maximum value on 8 May 2005. During the "Event"-period, the concentration of the accumulation mode was too low for a successful density analysis. The density for the Aitken mode increased during the "No event"-period and reached its maximum value during the "Event" - period. The highest density value for the Aitken mode was between 0.9 g/cm^3 – 1.3 g/cm^3. This indicates that the composition of the Aitken and the accumulation mode particles changed during the campaign. The composition could have changed due to the condensation of volatile species onto the particles.

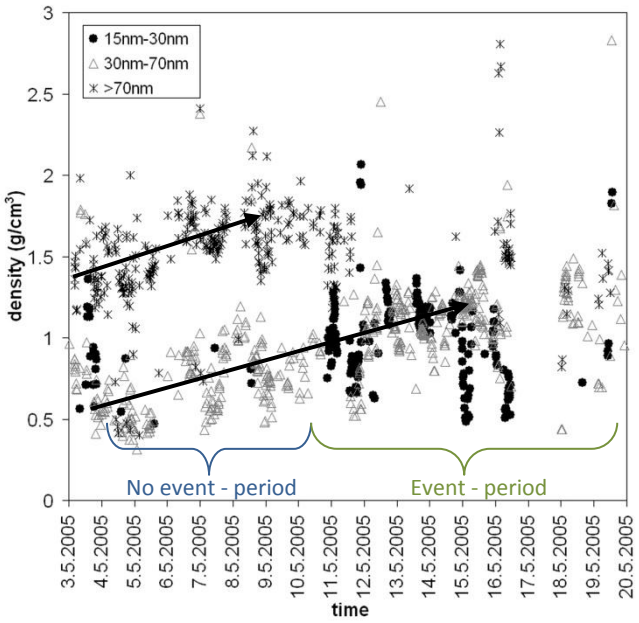

Figure 2.6. Density of nucleation (black dot), Aitken (grey triangle) and accumulation (black star) modes as a function of time. (Paper III)

The weather during the measurement campaign was typical Finnish springlike weather. Figure 2.7 presents the alterations in relative humidity (black stars), wind direction (grey triangles) and net radiation (grey lines) as a function of time. A decrease in relative humidity, an increase in net solar radiation and the turning of the wind turns toward north coincided with the increase in the density value of the Aitken mode (Fig. 2.6 and Fig. 2.7). This is an interesting result but a two-week measurement campaign is not long enough to make general conclusions about the dependence of density on weather parameters. Continuous measurements over a longer time period would be needed to establish the real reason for density changes.

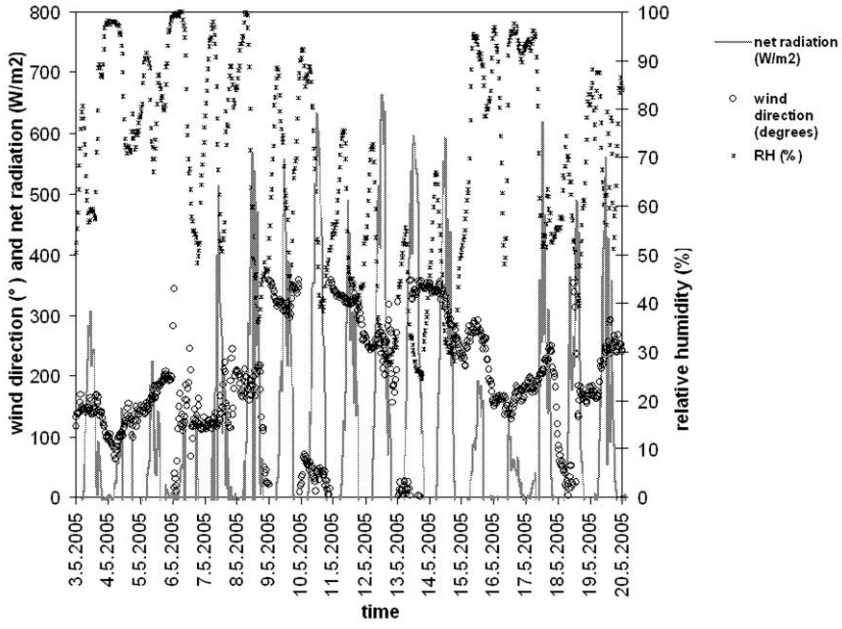

Figure 2.7. Weather parameters during the measurement campaign. Relative humidity (black star), wind direction (grey circle) and net radiation (grey line) are measured at SMEAR II station. (Paper III)

To be able to study the density of the nucleation mode, the particles need to generate a sufficient amount of current (20 % of total current). Generally, this condition can be

fulfilled during the new particle formation when the nucleation mode number concentration is high. Two different days have been selected for more detailed study. The first day is 4 May 2005, during which there was no nucleation mode present, and the particle size distribution stayed very stable. During another day 13 May 2005, an intense particle formation event was present and the concentration of the nucleation mode was high in the afternoon. The average values of main weather parameters and some gaseous components of air during the above mentioned days are presented in Table 2.3. The density values of the modes are presented in Figure 2.8c – d and the standard deviation of the results is analyzed with the method described in the end of section 2.1. Only the successful density analyzing results are presented in Figure 2.8 c – d. The corresponding mode GMD values are presented in Figure 2.8a – b. With a 5 % noise component added to the measured data, the density was evaluated 100 times. The error bar shown is the deviation of the 100 density values.

Table 2.3. Weather parameters on 4 and 13 May 2005 (Paper III)

4.5.2005	13.5.2005	units	parameters
5.9	10.4	◦C	Temperature
-0.006	-0.004	◦C	potential T gradient
86.7	38.9	%	RH
7.9	4.6	ppt	H_2O
115	196.2	◦	wind direction
5.1	14.69	W/m^2	UV-A
9.9	28.9	W/m^2	UV-A, during daytime
0.21	0.57	W/m^2	UV-B
0.43	1.2	W/m^2	UV-B, during daytime
36	175.4	W/m^2	Net Radiation
93.9	417.1	W/m^2	Net Radiation, during daytime
26.7	49.7	km	Visibility
1.61	0.73	ppb	NO_x
0.013	0.0004	ppb	NO
42.3	45.3	ppb	O_3
387	384.7	ppm	CO_2
0.1	0.08	ppb	SO_2

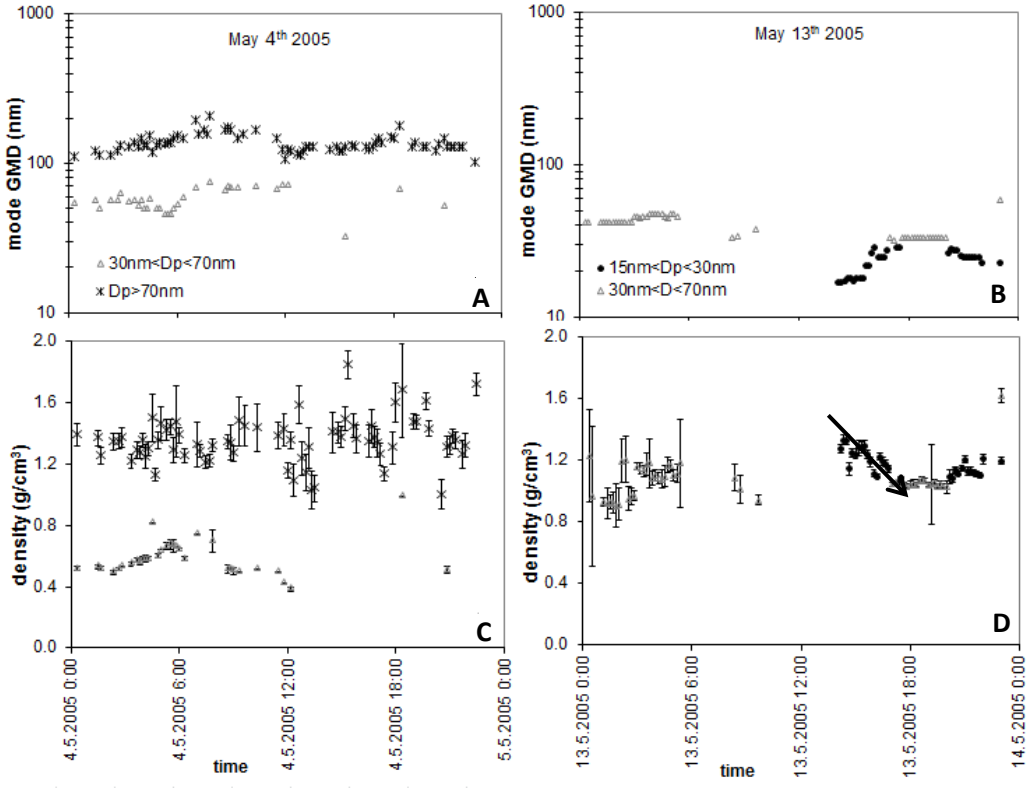

Figure 2.8. Mode GMD measured on 4 May 2005 (A) and 13 May 2005 (B) and the mode densities measured on 4 May 2005 (C) and 13 May 2005 (D). The arrows show the trend of the decreasing nucleation mode particle density during the growth process. (Paper III)

On 4 May (Fig. 2.8a), the particle population was very stable. In the evening, two concentration spikes occurred. The peaks were most likely some local pollutants, judging by the simultaneous NO_x and CO_2 concentration peak values. The density values for the Aitken (grey triangle) and the accumulation (black star) modes are very stable and the standard deviation was low. The density value for the Aitken mode was very low, 0.5 ± 0.2 g/cm^3 (Fig. 2.8c). The density of the accumulation mode was 1.4 ± 0.2 g/cm^3 and it remained very stable over the whole day. May 4th belongs to a "no - event"- period during which all the density values were low compared to the density values at the end of the measurement campaign. These low density values

can be explained with the results presented in the next chapters where the particle bounce in the ELPI impactor has been studied. The particle bounce produces an excess current to the lowest impactor stages. The density results are revisited in the Chapter 4 where the effect of particle bounce on the measurement results is studied.

On 13 May, new particle formation starts at noon (12:00) when the particle number concentration of the nucleation mode starts to increase. During the new particle formation event, the nucleation mode number concentration is very high and produces 20 % or more of the measured total current. On the other hand, the particle number concentration of the accumulation mode was too low for density estimation. The density value of the Aitken mode was 1.1 ± 0.2 g/cm^3 which is much higher than on 4 May. The density value of the nucleation mode was approximately 1.3 g/cm^3 when GMD was 17 nm. The density results of the nucleation mode are presented in Figure 2.8d. The density of the nucleation mode decreased as the mode GMD increased, indicating the condensation of some lighter compound than in the beginning of the formation. At 18:00, the nucleation mode particles reached the size of 33 nm and their density was 1.0 g/cm^3. At 19:30, the nucleation mode size decreased from 33 nm to 20 nm and particle density increased to 1.2 g/cm^3.

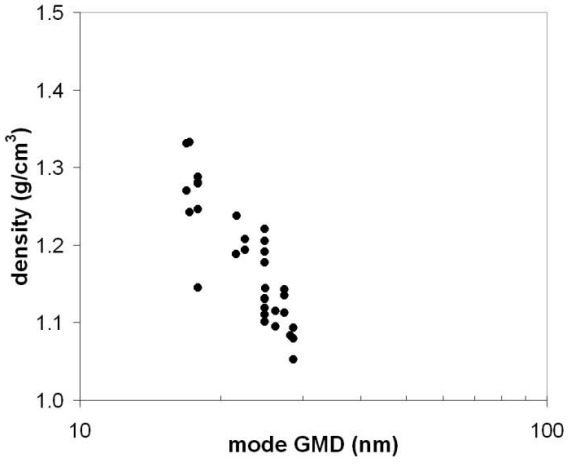

Figure 2.9. Density of the nucleation mode particles as a function of mode GMD during the growth process on 13 May (Paper III).

The density behavior of the nucleation mode during the growth process is illustrated with arrows (Fig 2.8 B and C). In Figure 2.9, the density values are presented as a function of mode GMD. It is clear from the figure that the density decreases as GMD is increases. The density of the condensing material can be estimated from Figure 2.9 by assuming spherical particles and calculating the change in particle mass during the growth process. In calculation, it was assumed that the change in particle size was the same as the change in mode GMD. According to the calculation, the density of the condensing material was 1.0 ± 0.2 g/cm^3 (Paper III).

3. Indication of solid SOA particles

Several weather parameters, such as solar radiation, temperature and relative humidity, may change simultaneously in boreal forest. These quantities can directly or indirectly affect the properties and the composition of SOA particles. It is therefore difficult to separate the effect of any specific parameter on particle density. Furthermore, the multimodal size distribution causes the density estimation of any single mode to be more sensitive to errors. In chamber measurements, the parameters can be controlled and the effects of specific parameters can be studied for a unimodal distribution.

The original purpose of the chamber measurements that will be presented in the next chapters was to study the density of SOA particles in a controlled environment. During the measurements, atypical ELPI currents were detected. The ELPI currents were bimodal even though the SMPS size distribution measured simultaneously was unimodal. The ELPI output showed currents in the channels corresponding to the real particle mode but also excess current in the lowest impactor stages (Fig. 3.1). When the greased smooth impactor collection plates were replaced with porous plates, the excess current disappeared and only the currents on the channels corresponding to the real particle mode remained (Fig. 3.1). The porous plates are frequently used to prevent bounce of solid particles in the impactor. It is apparent that the excess current was caused by particle bounce.

The particle density estimation method can produce a too low density values for a cases with particle bounce. For a single-mode distribution, the bounce could be

detected as a poor agreement between the simulated and the measured current values. However, for the multimodal case the implications could be more severe. For example, some of the nucleation and Aitken mode density results in Figure 2.6 are quite low. These low density results could be an artifact caused by particle bounce in the impactor. The density results of the boreal forest are revisited later in Chapter 5, but first certain even more important implications are treated.

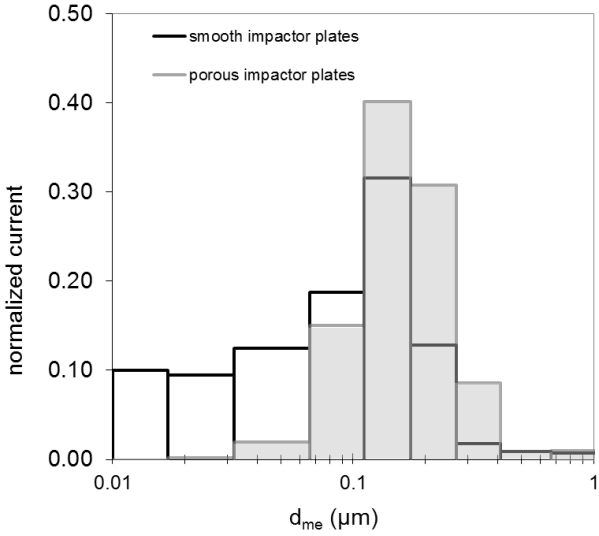

Figure 3.1. Measured ELPI currents using greased smooth impactor collection plates (white bars) and porous impactor collection plates (gray bars). (Adapted from Paper IV)

The particle bounce in an impactor is not a new finding. The bounce of particles has been studied previously by e.g. John W. 1995, Wall et al. 1990, Cheng and Yeh 1979. The general finding is that in a properly designed impactor, only solid particles bounce. Until recently, the SOA particles were assumed to be in the liquid state in atmospheric conditions (Marcolli et al. 2004, Pankow 1994, Odum et al. 1996). Therefore, the bounce of the SOA particles was an unexpected phenomenon. The excess current is a clear indication of solid particles and, on the next chapter (Chapter 4), the bounce of SOA particles is studied more closely.

4. Particle bounce and physical phase

4.1. Particle bounce in ELPI

In an impactor stage, particles of different size, shape, morphology and physical phase have different collection efficiencies. When a particle collides to an impactor collection plate, one part of the kinetic energy of the particle is dissipated in the deformation process, and another part is converted elastically to the kinetic energy of the rebound. A particle will bounce from the impaction collection plate if the rebound energy of the particle exceeds the adhesion energy. Thus, both the elastic properties of particles and the surface properties of the impactor collection plate affect the bouncing probability of particles (Rogers et al. 1984). Also relative humidity (RH) affects the bouncing probability as RH influences the viscoelastic properties of hygroscopic aerosol particles (Stein et al. 1994, Ehn et al., 2007). Overall, harder materials, larger particles or greater impact velocities will increase the bouncing probability in the impactor (John W. 1995). Furthermore, the greasing and the roughness of the impaction collection plate reduce the bouncing probability (Chang et al. 1999, Pak et al. 1992).

Easily deformed particles, for example liquid particles, usually tend to adhere to the impaction collection plates upon the collision, see Figure 4.1a. Solid particles can bounce from the impaction plate as their capture efficiency is smaller than that the efficiencies of easily deformed particles, Fig 4.1b. Usually, bouncing is an undesired phenomenon in the impactor because bouncing transfers larger particles to lower stages of the impactor and, therefore, causes a measurement artifact to the size distribution measurements. The bounce of particles can be hampered or prevented by using a porous impactor collection plate (Marjamäki and Keskinen, 2004), Fig. 4.1c. Often the greasing of smooth collection plate is enough to prevent the particle bounce (Pak et al. 1992).

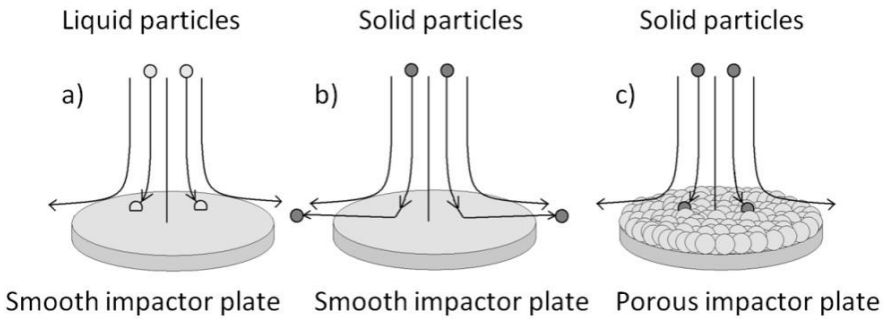

Figure 4.1. Particle behavior on the impactor collection plate. a) Liquid particles stick to an impactor plate. b) Solid particles can bounce from an impactor plate. c) Solid particles are captured to a porous impactor plate even if they would bounce from a smooth impactor plate.

The particle detection in the ELPI impactor is based on the electrical detection of particles. In the ideal case, a charged particle impacts onto the impactor collection plate and sticks. The impaction is measured as a current from the impactor stage using an electrometer (Fig. 4.2. a.). If the charged particle bounces from the impactor collection plate instead of sticking onto its surface, the bounced particle can either keep the charge or assign it to the surface. If the particle assigns the charge to the surface, the bounce is measured as a current from that impactor stage (Fig. 4.2. b.) although the particle continues to the next impactor stage. If the particle carries the charge further on, no current is measured (Fig. 4.2. c.). If a neutral particle bounces from the surface of the collection plate, the particle can also obtain a charge from the collection plate. In this case, negative current is measured (Fig. 4.2. d.) from that impactor stage.

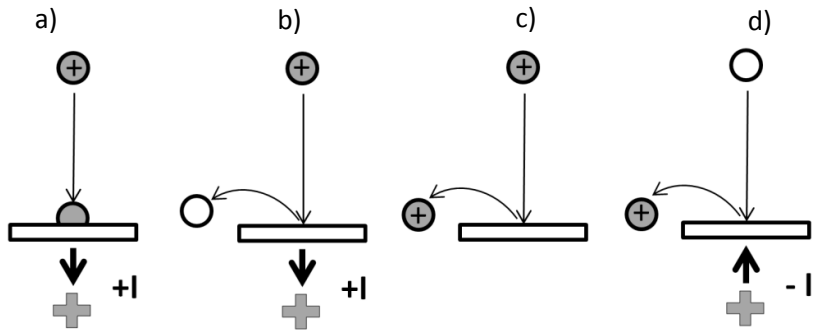

Figure 4.2. Behavior of a charged particle in the ELPI impactor collection plate and the measured current in different situations.

The study of particle bounce is not necessarily straightforward when both the bounce and the current transfer affect the measured currents. On the other hand, the current of the bounced particles provides also an opportunity to estimate charge transfer of particles. Instead of considering the bounce as an artifact, it can be used as a tool to study the physical state of particles.

4.2. Treatment of bounce data

Particle bounce can be detected from the excess current as described in the previous chapter (Fig. 3.1.) and particle bounce is a clear indication of the solidity of particles. The properties of particle bounce can also be studied in more detail. Next, two different methods to evaluate the particle bounce are presented. First, the bounce factor which describes the ratio between the excess current and the total current is introduced. Then, the procedure of bounce probability and charge transfer study is described.

Bounce factor

As an ad hoc quantity to describe particle bounce, the bounce factor is introduced. The bounce factor (BF_n) at different impactor stages (n) is based on the difference between the measured "bounced" currents and the simulated ideal currents. To clarify the names of the impactor stages used in this thesis, the filter stage is the stage 0, the new stage is the stage 1 and so on until the stage 12.

$$BF_n = \frac{\sum_{j=0}^{n-1} I_j - \sum_{j=0}^{n-1} I_j^{id}}{\sum_{j=n}^{12} I_j^{id}} \quad (4.1)$$

A tool to obtain the ideal simulated currents was readily at hand, as it is a part of the density estimation method (Ristimäki et al. 2002). In order to simulate the currents, the density of the particles is required. As the density estimation method is out of the question due to bouncing, the density value is derived by comparing the data from SMPS volume and AMS (Aerosol Mass Spectrometer, Aerodyne Inc.) mass size distributions (De Carlo et al., 2004). The amount of excess currents can be estimated by comparing the normalized measured currents (I) to the normalized simulated ideal currents (I^{id}). The density of particles used in the current simulation affects the value of the estimated excess current.

The described method is simple and very straightforward for analyzing particle bounce. The bounce factor does not represent any physical parameter of particles but describes the amount of current that is transferred to the lower impactor stages due to bounce.

Bounce probability and charge transfer

In this section, particle bounce in the impactor is treated using a simple model which takes into account the charge transfer during the impaction. The excess current can either be caused by the impaction of the bounced particle or by the charge transfer during the bounce. Therefore, the excess current can be described as a function of the bounce probability and the charge transfer term which both have a physical meaning. John W. (1995) describes the charge transferred q_T during the bounce of one particle as comprising of two independent processes:

$$q_T = q_C + \beta q_0 \,, \quad (4.2)$$

where q_C is the contact charge, q_0 is the precharge of the particle, and β is the fraction of precharge transferred to impactor stage. The first part, q_C, is assumed to be independent of the particle precharge q_0. The contribution of this part can be tested by turning the charger of the ELPI off. Figure 4.3 shows how the current of the stage 2 and the sum of the currents from 0 to 2 behave during such a test. During the *charger off* –period, the measured currents are less than 0.1% of the *charger on* –values. The fact that the sum of the currents is close to zero means that the average value of the precharge is zero. Incidentally, this also means that the SOA particles are in charge equilibrium. Probably most of the particles are neutral. Because the current from the stage 2 is zero, it can further assumed that the contribution of the contact charge process is negligible and, therefore, only the latter term of equation 4.2 is required to describe the transferred charge.

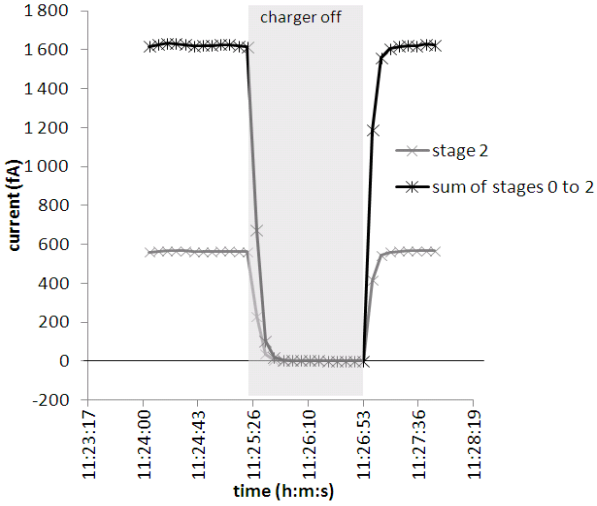

Figure 4.3. Current of stage 2 and sum of stages 0-2 during a *charger off* test. (Experiment B, GMD of 74 nm, see Table 4.1). (Paper VI)

In the case when the stage cut-point is clearly smaller than the mode GMD, it can be assumed that particles do not pass the stages without impacting on the impactor plates. In any stage *n*, a single particle will leave a charge of q_n, on average:

$$q_n = (1 - P_n)q_{0,n} + P_n\beta_n q_{0,n}\,, \tag{4.3}$$

where $q_{0,n}$ is the precharge of the particle (the charge of the particle entering the stage *n*) and P_n is the true bounce probability within the stage *n* and β_n is the fraction of precharge transferred to impactor stage *n*. The charge escaping the impactor stage with the bouncing particles is then

$$q_{0,n} - q_n = P_n(1 - \beta_n)q_{0,n}. \quad (4.4)$$

Multiplying both sides with NQ, where N is the particle number concentration entering the stage and Q is the volumetric flow rate provides the corresponding currents:

$$\sum_{j=0}^{n} I_j - I_n = P_n(1 - \beta_n)\sum_{j=0}^{n} I_j \quad (4.5)$$

Finally, by dividing the result the total current entering the stage yields the measured current penetration through the stage, or in other words the apparent bounce probability:

$$AP_n = \frac{\sum_{j=0}^{n} I_j - I_n}{\sum_{j=0}^{n} I_j} = P_n(1 - \beta_n) \quad (4.6)$$

4.3. Physical phase of SOA particles in the chamber and boreal forest

4.3.1. Measurements

The bounce and solidity of particles were studied both in a chamber and in a boreal forest. The physical state study in the boreal forest was conducted at the boreal forest measurement station, SMEAR II, in Hyytiälä. The measurement station is described in more detail in Section 2.2. The measurements in the boreal forest were performed with an Outdoor ELPI not included the new impactor stage. Therefore, the bounce factor studies were performed using the bounce factor calculated from stage 2 (BF_2). BF_2 means that the bounce factor has been calculated using the sum of currents of the impactor stages 0 and 1, see Eq. 4.1.

The chamber measurements were performed in the University of Eastern Finland. The measurement setup consisted of a chamber (made of FEP (Fluorinated ethylene propylene) film, volume 6m^3) (Hao et al. 2009) and the measurement systems for

gases and particles. The experiment runs are presented in Table 4.1. In these measurements, two different VOCs were used to produce the particles. No seed particles were used in the particle generation. Living Scots pine seedlings were used to produce natural biogenic VOCs and in addition also pure α-pinene was used to produce particles. The VOCs of living Scots pine represent natural atmospheric conditions and they consist of a large number of different organic compounds. One of the major VOCs released from the pine is α-pinene. The experiment runs where VOCs were produced by the living Scots pine are in two shades of green and the measurement runs performed with α-pinene are presented in two shades of gray, see Table 4.1.

Table 4.1. Description of the chamber experiment runs investigated in this thesis. The measurements with α-pinene are presented in two shades of gray and the measurements with living Scot pine are in two shades of green. The chamber was humidified prior to the experiment run and the temperature was 22 ± 1 ˚C.

Exp./ Paper	Description of experiment	RH %	VOC (ppb)	O_3 (ppb)	TME (ppb)	SO_2 (ppb)	density (g/cm^3)	ELPI (new impactor) impaction plate type
A / VI	α-pinene + O_3	30	7	35			1.1	smooth, greased foil
B / VI	α-pinene + O_3	30	45	43			1.1	smooth, greased foil
C	α-pinene + O_3	30	34	39			-	porous, greased
D	α-pinene + O_3	26	26	46			1.1 [#])	smooth
E / III IV	Pine + O_3	34	16.8	35			1.0	smooth, greased foil
F / III IV	Pine + OH +SO_2	31	108	35	35.2	22	1.1	smooth, greased foil *)

*) in experiment F, smooth greased plates were replaced with porous plates when the growth process was in a steady state situation.

[#]) The density is assumed to be the same as in the experiment runs A and B

The particle size distribution measurements were performed with two SMPSes (size ranges 3 – 60 nm and 10 – 700 nm), an ELPI (7 nm – 6 μm, with the new (17 nm cut-off size) stage) and an AMS (Aerosol Mass Spectrometer, Aerodyne Inc.). The density of particles was determined by comparing the SMPS volume and the AMS mass size

distributions (Hao et al. 2009). The analyzed density values are 1.0 g/cm^3 – 1.1 g/cm^3 which are higher than the bulk density of pure α-pinene (0.85 g/cm^3, CRC Physics) but lower than most analyzed effective density values for living Scotch pine (1.25 g/cm^3 Mentel et al. 2009, about 1.35 g/cm^3 Hao et al.2009). Kostenidou et al. 2007 reported lower density values for α-pinene SOA particles (0.9 g/cm^3 – 1.0 g/cm^3) indicating changes in particle morphology and solid or waxy physical state.

4.3.2. Bounce characteristics

Figure 4.4 shows the bounce factors (BF_1 to BF_4) calculated according to Eq. 4.1 for the experiment B. The curves show the values as a function of the GMD of the particle mode. First, all the curves increase with increasing GMD and, then, they seem to achieve a plateau. However, the plateau values differ between different stages, so that lower bounce factors are calculated for the stages with lower cut-sizes.

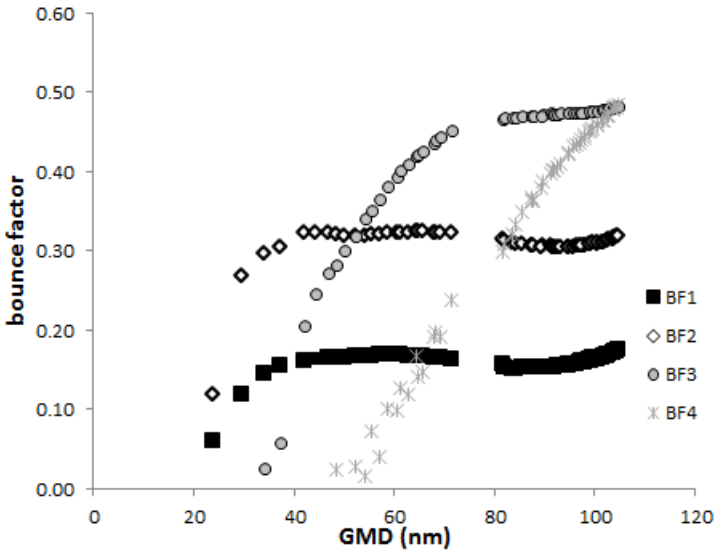

Figure 4.4. a) Bounce factors BF_1 to BF_4 (Eq. 4.1) as a function of mode GMD (Paper VI)

When moving towards the lower stages in the cascade impactor, the impactor jet velocity increases or, for the last stages, remains close to the sonic velocity of air

(Paper I). It is well known that when particle size is above the cutpoint diameter of the stage, the impaction velocity of the particles is close to the jet velocity (e.g. Cheng and Yeh 1979). This has been verified for the present impactor type by CFD (Computational Fluid Dynamics) modeling (Paper V, Arffman et al. 2011). Therefore, the actual bounce probability should increase or at least remain high as the particles bounce down to the lower stages of the impactor. Therefore, the lowering of the bounce factors for stages with lower cut-size diameters seems counter-intuitive.

Overall, if particle bounces from one impaction plate, it should be very probable that it would bounce from all the following plates as well. Finally, the particle should end up in the filter stage. Consequently, there should be excess current only in the filter stage if the bounced particles carried all their charge to the filter stage. Obviously, this is not the case. In addition to the particle bounce characteristics, also the particle charge transfer properties affect the excess current distribution observed at the lowest stages. In Figure 3.1, it can be seen that excess current is detected not only from the filter stage but from all the lowest stages.

Apparent bounce probabilities (Eq. 4.6) were calculated for the lowest impactor stages (i.e. *n* values of 1, 2, and 3) for several size distributions with GMD ranging from 85 nm to 100 nm (Paper VI). The values of bounce properties were different for different stages, but the values were rather constant for the studied GMD range. Table 4.2 shows the average values for each stage. As the precharge transfer term cannot be negative, the minimum value of β_n is zero. Therefore, the shown *AP* value is also the minimum value for the true bounce probability of the particles. The maximum of bounce probability *P* is one, which is also the maximum value for the precharge transfer term β. The precharge transfer term should be close to zero for insulating particles and close to unity for conducting particles. For sodium chloride the precharge transfer term has been measured to be 0.42 (John W. 1995). Most likely, the charge transfer term for the present case is nonzero and, thus, the true bounce probabilities are larger than the minimum values presented in Table 4.2.

Table 4.2. Maximum value of the fraction of particle precharge transferred during bounce, β(maximum) and apparent bounce probability, *AP* for the lowest impactor stages. The *AP* values are also the maximum bounce probability values for the same stages.

stage	β(maximum)	AP, P(minimum)
1	0.50	0.50
2	0.35	0.65
3	0.25	0.75

The effect of substrate

The measurements reported in Papers IV-VI were performed with greased impactor plates. In hindsight, particle bounce should generally be studied with both smooth and clean impactor plates. However, these were the first studies where bounce was detected with SOA particles. An example of the measurement of the bounce factor (BF_2) with three different substrates: bare smooth, greased foil and porous is presented in Figure 4.5. The particles in the experiment were α-pinene derived SOA particles generated in the chamber (see Table 4.1). The results in Figure 4.5 show that porous collection plated prevent the particle bounce and bare smooth impactor collection plates had the largest bounce factor, as was expected. The bounce efficiency on greased, smooth collection plates, on the other hand, could have depended on the thickness of the grease (Pak S. et al. 1992). All in all, in all the experiments presented in this thesis, the average bounce factor value (for particles larger than 40 nm) was almost the same (about 0.3). The value is only 40 % lower than the bounce factor measured without grease.

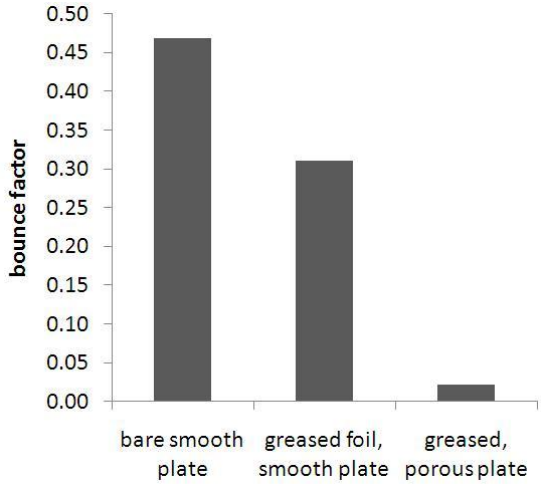

Figure 4.5. Average bounce factor for SOA particles in the size range of 40 nm – 100 nm, for different impactor plates. Bare smooth impactor plates (exp. D) yielded higher bounce compared to greased, smooth plates (exp. B). Nevertheless, the greasing did not fully prevent the bounce. The greased porous plates (exp. C), on the other hand, prevented the bounce (the bounce factor was almost zero).

4.3.3. Physical phase of SOA particles in the chamber and boreal forest

Figure 4.6 presents the bounce factor BF_2 as a function of mode GMD. The results represent a summary of several experiment runs (A, B, E, F and the boreal forest). The particles were formed in chamber conditions and in the boreal forest. The particles were derived of different VOCs and had different chemistry (with/without SO_2). All the SOA particles measured in the different situations had bounce factor larger than zero. Even the fresh particles (> 20 nm) had bounce factors larger than zero indicating that the particles are solid. The α-pinene and pine derived particles, with the same chemistry, behave almost identically. The bounce factor for particles produced by the pine with SO_2 (exp. F) or in the pinery is lower. The bounce factor seems to decrease when particle size decreases. This relationship is studied in more detail later on.

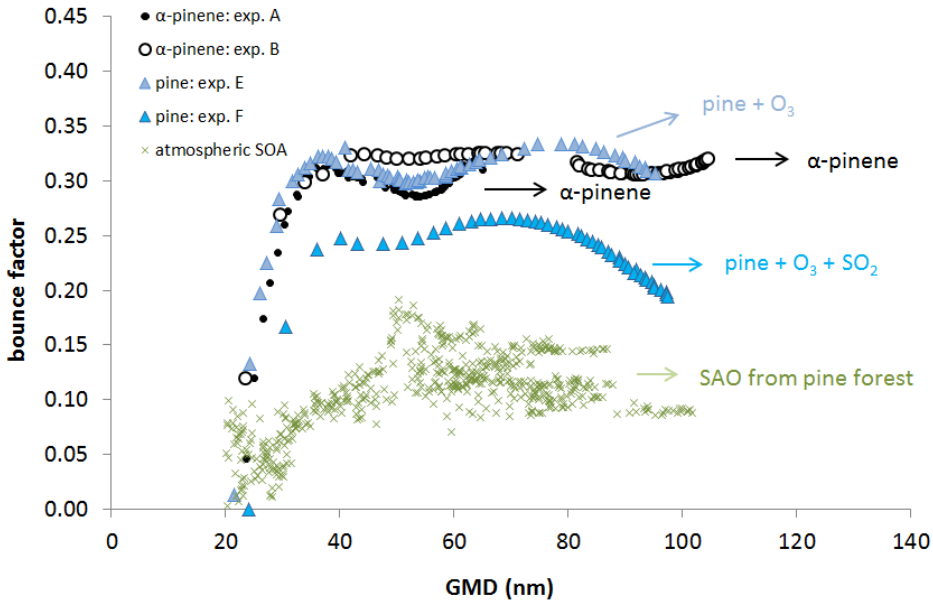

Figure 4.6. Bounce factor (BF_2) of pine derived SOA particles (blue triangles), α-pinene derived SOA particles (black and white dots) and SOA particles measured in the pinery (green cross).

The particles were also analyzed with a SEM. The electron microscopy samples were collected onto copper grids covered with holey carbon film. The sample aerosol flow was drawn through the grid by a flow rate of 0.2 Lpm (Lyyränen et al. 2009). The particles were collected by diffusion and at room temperature and pressure. The samples were analyzed using a field emission gun scanning electron microscope (FEG-SEM, Zeiss ULTRAplus; detector: inlense SE; acceleration voltage: 2 kV). The particle size and size distribution analyses from SEM figures were performed with the semi-automatic and custom made Matlab®-base analysis presented by Hirvonen et al. 2005.

The SEM figures can be seen in Figures 4.7 (for pine, exp. E and F in Table 4.1) and 4.8 (for α-pinene, exp. C in Table 4.1). The figures show that measured SOA particles are almost spherical but also some edges and irregular shapes exist. In Figure 4.7a, a small agglomerate can be seen. If the particles had been in the liquid phase, the particles would have coalesced to form a single larger particle. The particle size distribution was analyzed from the SEM-pictures and compared to the size distributions measured

during the SEM sample collections with the SMPS. The size distributions were very similar to each other indicating that particles were neither substantially evaporated nor flattened and that the SEM samples were representative to the aerosol. For comparison, liquid DOS particles were also collected and analyzed with the SEM, and clear irregularly shaped pools of coalesced particles were detected (Paper IV). The collected SOA particle sample was analyzed also with a TEM (transmission electron microscope). The TEM showed no indications of a crystalline structure in the electron diffraction pattern (Paper IV).

As a summary, a clear bounce tendency of the particles in the impactor, shown as excess current in the lowest stages and a nonzero bounce factor, suggest that the measured particles were not in the liquid state. The presented SEM figures show agglomerate particles and, further, particles with edges and irregular shapes which are typical for solid particles. No crystalline structure was found for the SOA particles in TEM analysis. All the above mentioned observations support the explanation that the SOA particles were in a glassy solid phase.

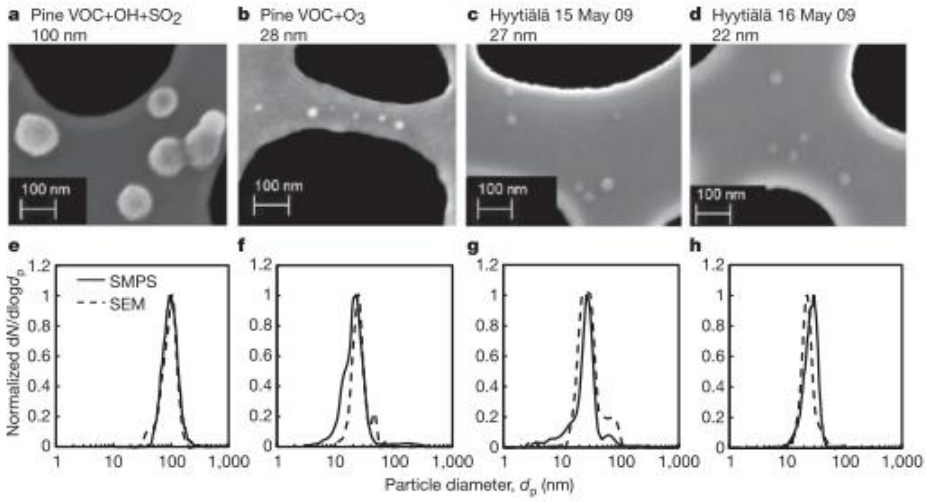

Figure 4.7. First pictures of pine derived SOA particles. In the upper line, analyzed SEM samples of pine experiments. In the lower line, the measured SMPS size distributions and the size distributions based on SEM-figure analyzes (Paper IV). a) Pine VOC+OH+SO2 is experiment F and b) Pine VOC+O3 is experiment E, see Table 4.1.

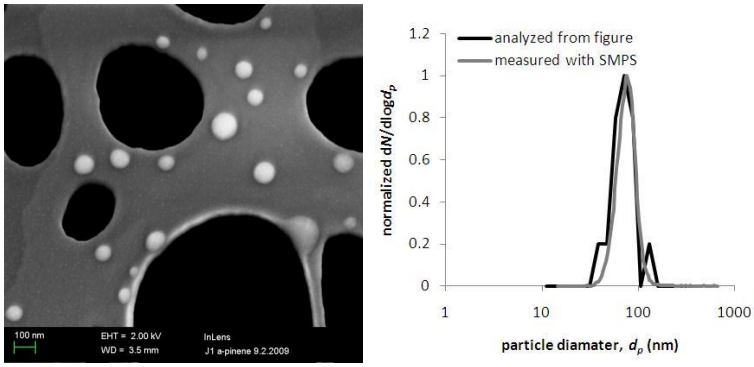

a) b)

Figure 4.8. (a) SEM-picture of SOA particles formed by ozonolysis of pure α-pinene (exp C, Table 4.1). The size bar is 100 nm. The particles are almost spherical but they also have some irregular shapes. (b) The size distribution analyzed from the SEM-image and SMPS size distribution measured during SEM sample collecting. (adapted form Paper VI)

Changes in the bounce factor

Figure 4.9 shows the bounce factor curves of Figure 4.4 normalized by dividing the individual BF_n values by the highest value of the corresponding BF_n curve of Figure 4.4. The GMD values are normalized in Figure 4.9 by dividing individual GMD values by the cutpoint diameter of the corresponding impactor stage (*n*). The bounce factors from BF_2 to BF_4 all decrease rapidly approximately at value one in normalized GMD. This is probably an instrument effect and it can be readily explained by the impactor operation characteristics. As particle size decreases close to the stage cutpoint diameter, the collision velocity of the particles on the impactor plate decreases. At cutpoint diameter, 50% of the particles do not even collide with the plate. Thus, by definition, the median collision velocity at cutpoint is zero. According to various fundamental studies of particle bounce, bounce probability decreases with decreasing collision velocity (John W. 1995). This has been shown in various impactor bounce studies as a local maximum in the collection efficiency for particle sizes of approximately the cutpoint diameter. Therefore, it is evident that the rapid decrease in the bounce factor curves for the distributions having GMDs close to the stage cutpoint does not represent any changes in particle properties but is an inherent property of the measurement device.

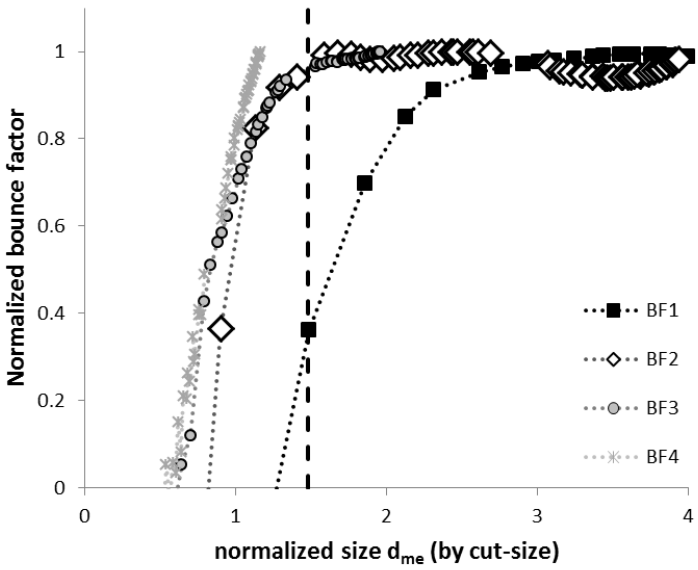

Figure 4.9. Normalized bounce factors as a function of normalized GMD. (Paper VI)

However, the normalized BF values presented as a function of normalized GMD in Figure 4.9 reach a plateau soon above unity. This reflects the fact that the median collision velocities reach values high enough for the bounce values to become practically constant. Here, the normalized GMD value of 1.5 is chosen as an estimate for this to occur. In other words, for the stages from 2 to 4, the normalized BF values for the GMD values above 1.5 times the cutpoint diameter are expected to be free of the instrument effect. This limit is shown by the dashed vertical line in Figure 4.9.

For the impactor stage 1, the 1.5 times the corresponding cutpoint value is approximately 25 nm. Figures 4.4 and 4.9 show that the BF_1 starts to decrease at GMD values well above this value. From the geometrical and flow dynamical points of view, the result of the lowest impactor stage is quite similar to the other ones in Figure 4.9. Further, the jet velocity at the stage is not lower than at higher stages. The basic difference between the stages is that the pressure and, consequently, the cutpoint diameter decrease as stage numbering decreases. This result indicates that the decrease in the bounce factor of the smallest particles, which bounce for the first time in the 1st impactor stage, is caused by changes in the particles physical properties, not by the instrument functions.

The bounce factor involves the calculation of the simulated (ideal) current values for the impactor stages. The simulated current values depend on the assumed values for particle density. The underestimation of density produces a too low bounce factor. Therefore, the lowering of the bounce factor for the smallest particles could partly be caused by an increase in the density of the particles. However, realistic particle density values (here assumed to be in the range from 0.8 g/cm^3 to 2.0 g/cm^3) cannot fully explain the decrease in the bounce factor for the smallest particles.

In all the experiments presented in this thesis, the bounce factor decreased when GMD decreased. The decrease cannot be explained as a mere instrument effect. Possibly the small particles have different composition and, therefore, a different physical phase or otherwise different bounce or charge transfer characteristics. Another example of the possible composition dependent bounce factor is shown in Figure 4.6. Through the particle growth process in the experiment E (pine + SO_2 + O_3 (+TME)), the bounce factor was lower than in the pine experiments containing no SO_2 (Fig. 4.6).

All the factors affecting the bounce factor are presented in the graph (Fig. 4.10.). The chemical composition of particles can change due to condensation or chemical reactions. The change in chemical composition can change the particle bounce but also the charge transfer ability and density. Further, the density can change the bounce factor due to the calculation procedure.

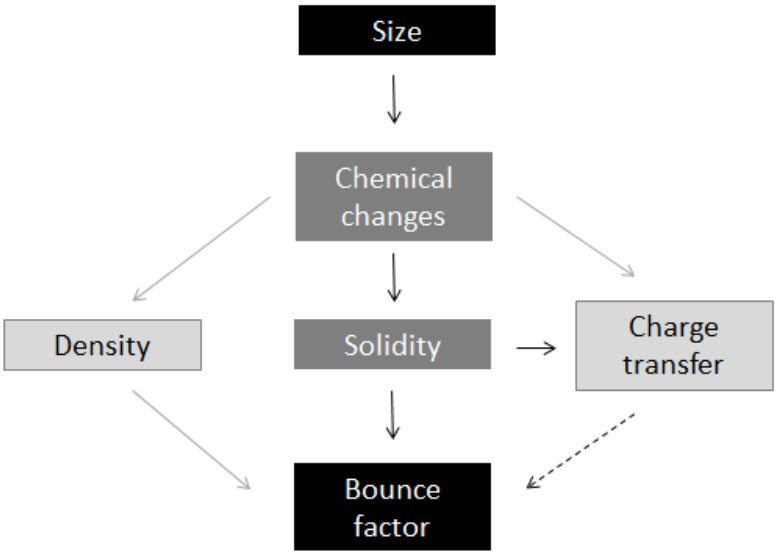

Figure 4.10. Graph of parameters that affect the bounce factor

The observation that SOA particles consist of an amorphous solid phase is a new and important finding. The result improves our understanding both on the formation of SOA particles and on the mechanisms by which they affect different physical and chemical processes in the atmosphere.

The formation mechanism of solid SOA particles from Scots pine, boreal forest or α-pinene is not well known. The solid particulate matter can be formed straight from gaseous components by nucleation (Wagner et al. 2011) or the original nucleation may produce liquid particles which in turn will go through a phase transition from the liquid phase to amorphous solid (Zorbis et al. 2008).

The observed solidity of the particles can influence the hygroscopic properties of aerosol particles and, therefore, their ability to accommodate water and act as cloud condensation nuclei or as ice nuclei, reduce the rate of heterogeneous chemical reactions and eventually alter the atmospheric lifetime of particles (Paper IV). The observation presented in this thesis challenges the traditional views on the kinetics and thermodynamics of SOA formation, their transformation in the atmosphere and their implications on air quality and climate. In Figure 4.11, the implications of the

solidity of SOA particles are presented in a structural way in order to describe how our understanding on particle behavior in the atmosphere should be updated.

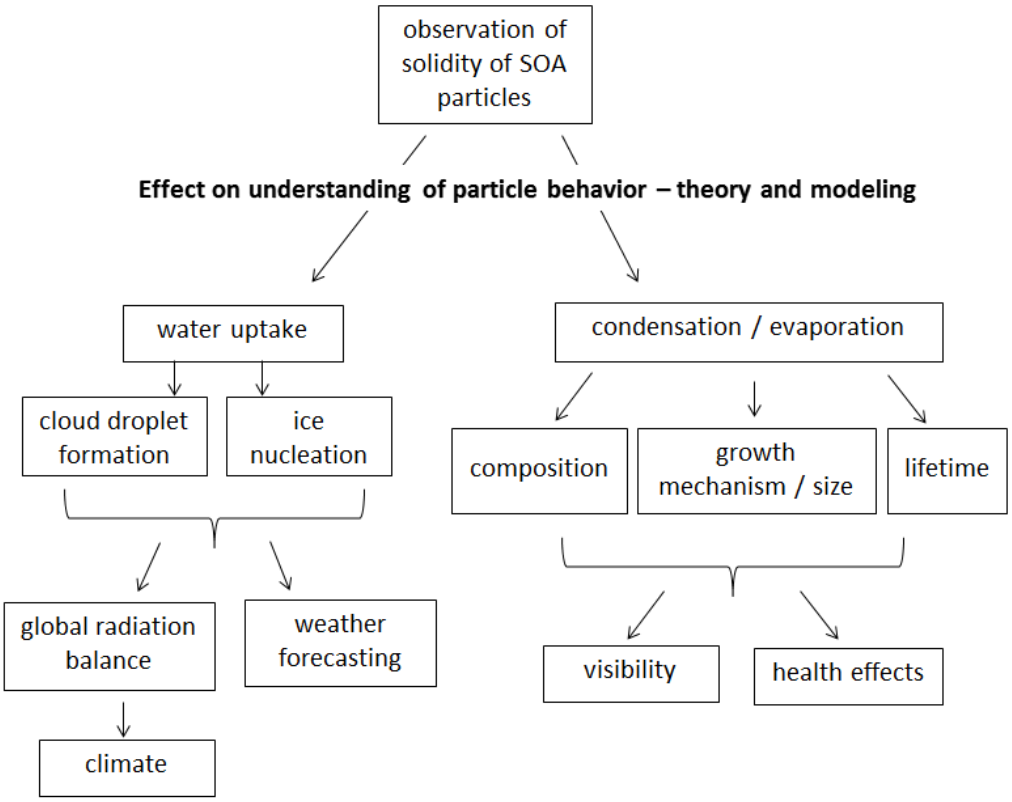

Figure 4.11. Implications of solidity of SOA particles for the understanding of particle behavior in the atmosphere

5. Revisiting the density analyzing results

As evident from above, the boreal forest SOA particles can bounce in the impactor (Fig. 4.6). The particle bounce causes excess current to the lowest impactor stages and, furthermore, affects the density estimation routine. Here, the effect of particle bounce on the density estimation results presented earlier is shortly discussed.

The measured density values of the accumulation mode are most likely correct. The results agree well with the results of Saarikoski et al. (2005). The density results of the

nucleation and Aitken mode cannot be completely trusted until new measurements with porous impactor plates have been conducted or some other confirmation of the density has been obtained. Especially the very low density values (< 0.7 g/cm^3) are most probably an instrument artifact caused by particle bounce.

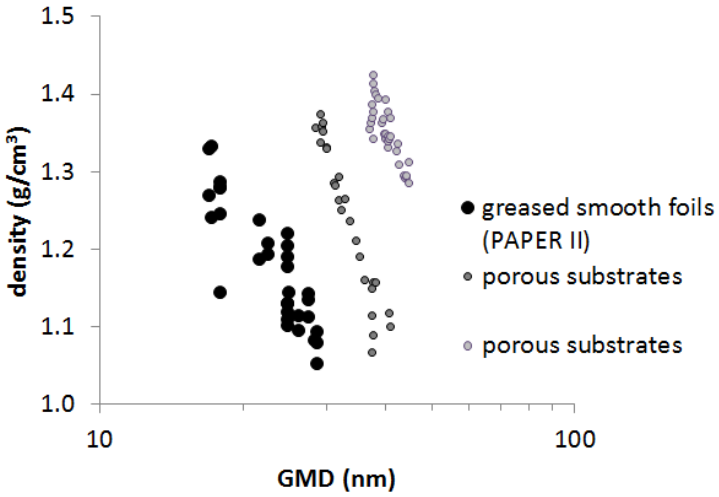

Figure 5.1. Density of nucleation mode particles in a boreal forest measured with smooth (black dot) and porous impactor plates (gray dots).

Further, particle bounce could cause the decreasing density for the nucleation mode particles during particle growth, such as shown in Fig. 2.9. There is some indication, however, that the decrease in the density can also be real. Figure 5.1 presents the density values shown in Figure 2.9 together with the density values calculated from the data of a short measurement campaign using porous impactor plates. The density values differ for different events, but they are in the same range and, further, all values decrease during particle growth. The measured density reaches values that are rather low, but density values of (0.9 g/cm^3 – 1.0 g/cm^3) have occasionally been reported for SOA particles (Kostenidou et al., 2007). Hao et al. 2009 reported indication of size dependence density values in Aitken mode but not in accumulation mode. In any case, a longer measurement campaign with porous impactor plates should be arranged to study the density values of the nucleation and Aitken mode particles.

Conclusions

In this thesis, the ELPI impactor was modified to be suitable for smaller particles and the density estimation method was improved to be suitable for smaller particle sizes. The data treatment of the method was modified to be suitable for large data series and multimodal size distributions which both are typical for atmospheric aerosol measurements. Atmospheric aerosol measurements have been performed at the SMEAR II station in a boreal forest. The density of nucleation, Aiken and accumulation modes was measured. The density estimation for accumulation mode particles was in agreement with the results obtained with a mass closure analysis. The obtained density estimation of nucleation and Aitken mode particles can be lower than the real due to the excess current formed by particle bounce in the impactor. The confirmation measurements in the boreal forest using porous substrates indicate that the density of nucleation particles really decreases during the growth process. Nevertheless, a longer measurement campaign is required in order to be able to analyze the density of nucleation and Aitken mode particles in different conditions. The density analyzing method itself is suitable for atmospheric measurements but particle bounce in the impactor needs to be prevented. This can be accomplished by using porous substrates. However, the porous substrates impair the impactor size segregation (Marjamäki and Keskinen, 2004) and, in multimodal size distributions, this results in more noise in the density results.

Further, the bounce behavior of SOA particles was studied using the ELPI impactor. The particles were observed to bounce from smooth impaction plates towards the lower impactor stages, indicating a solid or semi-solid physical state. According to the results, the SOA particles formed by ozonolysis of pure α-pinene had similar bouncing ability as the living Scots pine derived particles. This indicates that the phase behavior of the α-pinene derived SOA particles is comparable to the phase behavior of the pine derived SOA particles in chamber measurements. Therefore, α-pinene appears to be a good model component for the pine emitted VOCs when the physical properties of the particles are considered. It is even possible that α-pinene derived oxidation products are the ones responsible for the solidification behavior of the SOA particles produced by boreal forests. SO_2 addition was found to decrease the bounce of the formed particles. This indicates that different chemical composition of the particles affects the bounce. The SOA particles in the boreal forest bounced in the ELPI impactor indicating solid particles. The particles' solidity was also confirmed in the

SEM and TEM analyses. Based on the impactor bounce results and SEM and TEM analyses, the SOA particles in the boreal forest and in the chamber measurements can form an amorphous glassy solid particle state.

The measured bounce factor of particles larger than 40 nm did not significantly change during the particle growth process indicating no changes in particle solidity in this size range. On the other hand, for the smallest particles the calculated bounce factor showed clear changes: the amount of bounce increased as particle size increased. This indicates that particles become more solid during their early growth/ageing process.

The maximum value of the bounce factor decreased along with the impactor stages. A simplified model to describe charge transfer behavior in the bounce process was presented. According to the model, the measured values can be explained by a combination of bounce probability and charge transfer between the particles and the impaction surface. The results can be explained if at least 50 % of the particles bounce from the impactor plates. The value is quite independent of particle diameter once the diameter is well above the impactor stage cutpoint diameter.

After first indication that SOA particles are form solid particles in atmospheric conditions, related and supporting studies have been published. The work has just begun but it starts to become clear that SOA particles can really be solid. Since, for example, water uptake or evaporation of solid particles can be very different compared to liquid particles these new results of SOA particles' properties can provide an opportunity to improve the models of particle behavior in the atmosphere.

References

Arffman, A., Marjamäki, M., Keskinen, J., Simulation of Low Pressure Impactor Collection Efficiency Curves, *J. Aerosol Sci*., 42, 329-340, 2011.

Chang M., Kim, S., Sioutas, C., Experimental studies on particle impaction and bounce effects of substrate design and materials, *Atmos. Environ*. 33, 2313-2322, 1999.

Cheng Y.-S., Yeh H.-C., Particle bounce in cascade impactors, *Environ. Sci. Technol*., vol 13, 11, 1392-1395, 1979.

Cozic, J., Verheggen, B., Weingartner, E., Crosier, J., Bower, K., Flynn, M., Coe, H., Henning, S., Steinbacher, M., Collaud Coen, M., Petzold, A., Baltensperger, U.: Chemical composition of free tropospheric aerosol for PM1 and coarse mode at the high alpine site Jungfraujoch*, Atmos. Chem. Phys*., 8, 407-423, 2008.

CRC Handbook of Chemistry and Physics, 87th Edition

Cross, E.S., J.G. Slowik, P. Davidovits, J.D. Allan, D.R. Worsnop, J.T. Jayne, D.K. Lewis, M. Canagaratna, and T.B. Onasch (2007). Laboratory and ambient particle density determinations using light scattering in conjunction with aerosol mass spectrometry. Aerosol Science and Technology, 41(4): 343-359

De Carlo, P.F., Slowik, J.G., Worsnop, D.R., Davidovits, P., and Jimenez, J.L., Particle morphology and density characterization by combined mobility and aerodynamic diameter measurements. Part 1: Theory, *Aerosol. Sci. Technol*., 38, 1185-1205, 2004.

Ebben, C. J., Martinez, I. S., Shrestha, M., Buchbinder, A. M., Corrigan, A. L., Guenther, A., Karl, T., Petäjä, T., Song, W. W., Zorn, S. R., Artaxo, P., Kulmala, M., Martin, S. T., Russell, L. M., Williams, J., and Geiger, F. M. (2011) Contrasting organic aerosol particles from boreal and tropical forests during HUMPPA-COPEC-2010 and AMAZE-08 using coherent vibrational spectroscopy, Atmos. Chem. Phys., 11, 10317-10329, doi:10.5194/acp-11-10317-2011, 2011

Ehn, M., Petäjä, T., Aufmhoff, H., Aalto, P., Hämeri, K., Arnold, F., Laaksonen, A., and Kulmala, M.: Hygroscopic properties of ultrafine aerosol particles in the boreal forest: diurnal variation, solubility and the influence of sulfuric acid, *Atmos. Chem. Phys*., 7, 211-222, 2007

Hallquist M., Wenger J. C., Baltensperger U., Rudich Y., Simpson D., Claeys M., Dommen J., Donahue N. M., George C., Goldstein A. H., Hamilton J. F., Herrmann H., T. Hoffmann, Iinuma Y., Jang M., Jenkin M. E., Jimenez J. L., Kiendler-Scharr A., Maenhaut W., McFiggans G., Mentel Th. F., Monod A., Prévôt A. S. H., Seinfeld J. H., Surratt J. D., Szmigielski R., and Wildt J., 2009. The formation, properties and impact of secondary organic aerosol: current and emerging issues, *Atmos. Chem. Phys.*, 9, 5155-5236.

Hao, L. Q., Yli-Pirilä, P., Tiitta, P., Romakkaniemi, S., Vaattovaara, P., Kajos, M. K., Rinne, J., Heijari, J., Kortelainen, A., Miettinen, P., Kroll, J. H., Holopainen, J. K., Smith, J. N., Joutsensaari, J., Kulmala, M., Worsnop, D. R. and Laaksonen, A. New particle formation from the oxidation of direct emissions of pine seedlings, *Atmos. Chem. Phys*., 9, 8121-8137, 2009.

Hari P., Kulmala L., *Boreal Forest and Climate Change*, p. 412, 2009.

Hirvonen, P., Huttunen, H. & Lappi, M. Estimatin the distibution of Particle dimensions for electron microscope images, In: Dougherty, E. R., Astola, J. T. & Egiazarian, K. O. (eds.). Proceedings of SPIE and IS&T Ekectron Imaging, Image Processing: Algorithms and Systems IV, San Jose, California, USA, 17-18 January 2005, pp. 248-256, 2005.

Hu M., Peng J., Sun K., Yue D., Guo S., Wiedensohler A., Zhijun W, Estimation of Size-resolved Ambient Particle Density Based on the Measurement of Aerosol Number, Mass and Chemical Size Distributions in the Winter of Beijing. *Environ. Sci. Technol*., Just Accepted Manuscript. DOI: 10.1021/es204073t. Publication Date (Web): March 29, 2012

Hussein, T., Dal Maso, M., Petaja, T., Koponen, I.K., Paatero, P., Aalto, P.P., Hämeri, K., Kulmala, M.: Evaluation of an automatic algorithm for fitting the particle number size distributions, *Boreal Environ. Res.*, 10, 337-355, 2005.

John Walter, Particle-Surface Interactions:Charge Transfer, Energy Loss, Resuspension, and Deagglomeration, *Aerosol Sci. Technol.*, 23, 2-24, 1995.

Kanakidou M., Seinfeld J. H., Pandis S. N., Barnes I., Dentener F. J., Facchini M. C., Van Dingenen R., Ervens B., Nenes A., Nielsen C. J., Swietlicki E., Putaud J. P., Balkanski Y., Fuzzi S., Horth J., Moortgat G. K., Winterhalter R., Myhre C. E. L., Tsigaridis K., Vignati E., Stephanou E. G., and Wilson J. 2005. Organic aerosol and global climate modelling: a review. *Atmos. Chem. Phys*. 5: 1053-1123.

Keskinen J., Pietarinen K., Lehtimäki M., Electrical low pressure impactor, *J. Aerosol Sci. Technol.*, 17, 199-212, 1992.

Keskinen, J., Marjamäki M., Virtanen A., Mäkelä T., Hillamo R.: Electrical Calibration Method for Cascade Impactors. *J. Aerosol Sci*., 30, 111-116, 1999.

Kostenidou, E., Pathak, R. K., and Pandis, S. N.: An algorithm for the calculation of secondary organic aerosol density combining AMS and SMPS data, *Aerosol Sci. Tech*., 41, 1002–1010, 2007.

Kulmala, M., Hämeri, K., Aalto, P.P., Mäkelä, J.M., Pirjola, L., Nilsson, E.D., Buzorius, G., Rannik, U., Dal Maso, M., Seidl, W., Hoffman, T., Janson, R., Hansson, H.C., Viisanen, Y., Laaksonen, A., O'Dowd, C.D.: Overview of the international project on biogenic aerosol formation in the boreal forest (BIOFOR), *Tellus*, 53B, 324-343, 2001.

Kulmala, M., Vehkamäki, H., Petäjä, T., Dal Maso, M., Lauri, A., Kerminen, V.-M., Birmili, W. and McMurry, P. H., Formation and growth rates of ultrafine atmospheric particles: A review of observations, *J. Aerosol Sci*. 35, 143-176, 2004.

Kulmala, M., Asmi, A., Lappalainen, H. K., Baltensperger, U., Brenguier, J.-L., Facchini, M. C., Hansson, H.-C., Hov, Ø., O'Dowd, C. D., Pöschl, U., Wiedensohler, A., Boers, R., Boucher, O., de Leeuw, G., Denier van den Gon, H., Feichter, J., Krejci, R., Laj, P., Lihavainen, H., Lohmann, U., McFiggans, G., Mentel, T., Pilinis, C., Riipinen, I., Schulz, M., Stohl, A., Swietlicki, E., Vignati, E., Amann, M., Amann, M., Alves, C., Arabas, S., Artaxo, P., Beddows, D. C. S., Bergström, R., Beukes, J. P., Bilde, M., Burkhart, J. F., Canonaco, F., Clegg, S., Coe, H., Crumeyrolle, S., D'Anna, B., Decesari, S., Gilardoni, S., Fischer, M., Fjæraa, A. M., Fountoukis, C., George, C., Gomes, L., Halloran, P., Hamburger, T., Harrison, R. M., Herrmann, H., Hoffmann, T., Hoose, C., Hu, M., Hõrrak, U., Iinuma, Y., Iversen, T., Josipovic, M., Kanakidou, M., Kiendler-Scharr, A., Kirkevåg, A., Kiss, G., Klimont, Z., Kolmonen, P., Komppula, M., Kristjánsson, J.-E., Laakso, L., Laaksonen, A., Labonnote, L., Lanz, V. A., Lehtinen, K. E. J., Makkonen, R., McMeeking, G., Merikanto, J., Minikin, A., Mirme, S., Morgan, W. T., Nemitz, E., O'Donnell, D., Panwar, T. S., Pawlowska, H., Petzold, A., Pienaar, J. J., Pio, C., Plass-Duelmer, C., Prévôt, A. S. H., Pryor, S., Reddington, C. L., Roberts, G., Rosenfeld, D., Schwarz, J., Seland, Ø., Sellegri, K., Shen, X. J., Shiraiwa, M., Siebert, H., Sierau, B., Simpson, D., Sun, J. Y., Topping, D., Tunved, P., Vaattovaara, P., Vakkari, V., Veefkind, J. P., Visschedijk, A., Vuollekoski, H., Vuolo, R., Wehner, B., Wildt, J., Woodward, S.,

Worsnop, D. R., van Zadelhoff, G.-J., Zardini, A. A., Zhang, K., van Zyl, P. G., Kerminen, V.-M., S. Carslaw, K., and Pandis, S. N.: General overview: European Integrated project on Aerosol Cloud Climate and Air Quality interactions (EUCAARI) – integrating aerosol research from nano to global scales, *Atmos. Chem. Phys*., 11, 13061–13143, 2011.

Lyyränen, J., Backman, U., Tapper, U., Auvinen, A., and Jokiniemi, J. A size selective nanoparticle collection device based on diffusion and thermophoresis, *Journal of Physics: Conference Series*, 170, 012011 (11pp), 2009.

Maenhaut, W., Jaffrezo, J.-L., Hillamo, R.E., Mäkelä, T., and Kerminen, V.-M.: Size-fractionated aerosol composition during an intensive 1997 summer field campaign in northern Finland, Nucl. Instrum. Methods, B150, 345-349, 1999.

Marcolli, C., Luo, B. P. & Peter, T. Mixing of the organic aerosol fractions: liquids as the thermodynamically stable phases*. J. Phys. Chem*. A 108, 2216–2224, 2004.

Marjamaki M, Keskinen J, Chen D.R., Pui D.Y.H.: Performance evaluation of the electrical low-pressure impactor (ELPI), *J. Aerosol Sci.,* 31, 249-261, 2000.

Marjamäki, M., Ntziachristos, L., Virtanen, A., Ristimäki, J., Keskinen, J., Moisio, M., Palonen, M., Lappi, M., Electrical filter stage for the ELPI, *Society of Automotive Engineers (SAE) Technical paper series* 2002-01-0055, 2002.

Marjamäki M., Keskinen J., Estimation of the Cutpoint of an Impactor with Porous Substrates, *J. Aerosol Sci.*, 35, 657-663, 2004

Mc Murry P., Wang X., Park K., Ehara K., The relationship between mass and mobility for atmospheric particles: A new technique for measuring particle density, *Aerosol Sci. Tech.*, 36, 227-238, 2002.

Mentel, Th.F., Wildt, J., Kiendler-Scharr, A., Kleist, E., Tillmann, R., Dal Maso, M., Fisseha, R., Hohaus, Th., Spahn, H., Uerlings, R., Wegener, R., Griffiths, P.T., Dinar, E., Rudich, Y., and Wahner, A.: Photochemical production of aerosols from real plant emissions, *Atmos. Chem. Phys*., 9, 4387–4406, 2009.

Mäkelä J. M., Aalto P., Jokinrn V., Pohja T., Nissinen A., Palmroth S., Markkanen T., Seitsonen K., Lihavainen H., Kulmala M., Observations of ultrafine aerosol particle formation and growth in boreal forest*, Geophys. Res. Lett*., 24, 1291-1222, 1997.

Mäkelä J. M., Koponen I., Aalto P., Kulmala M., One-year data of submicron size modes of tropospheric background aerosol in southern Finland, *J. Aerosol Sci*., 31, 595-611, 2001.

Odum, J. R., Hoffmann, T., Bowman, F., Collins, D., Flagan, R. C., and Seinfeld, J. H.: Gas/particle partitioning and secondary organic aerosol yields, *Environ. Sci. Technol*., 30, 2580–2585, 1996.

Pak S. S., Liu B. Y. H., Rubow K. L., Effect of coating thickness on particle bounce in inertial impactors, *Aerosol Sci. Technol*., 16, 141-150, 1992.

Pankow J.F., An absorption model of the gas/aerosol partitioning involved in the formation of secondary organic aerosol. *Atmos. Environ*., 28, 189-193, 1994.

Putaud, J.-P., Van Dingenen, R., Dell'Acqua, A., Raes, F., Matta, E., Decesari, S., Facchini, M.C., and Fuzzi, S.: Size-segregated aerosol mass closure and chemical composition in Monte Cimone (I) during MINATROC, *Atmos. Chem. Phys.,* 4, 889–902, 2004.

Ristimäki, J., Virtanen, A., Marjamäki, M., Rostedt, A., Keskinen J.: On-line measurement of size distribution and effective density of submicron aerosol particles. *J. Aerosol Sci*., 33, 1541-1557, 2002.

Rogers, L.N., and Reed, J., The adhesion of particles indergoing elastic-plastic impact with a surface. *J.Phys D: Appl. Phys.* 17, 677-689, 1984.

Saarikoski S., Mäkelä T., Hillamo R., Aalto P., Kerminen V.-M., Kulmala M., Physico-Chemical characterization and mass closure of size-segregated aerosols in Hyytiälä, Finland, *Boreal Environ. Res*., 10, 358-400, 2005.

Seinfeld, J. H., and Pandis, S. N.: *Atmospheric chemistry and physics*. From air pollution to climate change. John Wiley & Sons, New York, 1998.

Smith, J.N., Moore, K.F., Eisele, F.L., Voisin, D., Ghimire, A.K., Sakurai, H., McMurry, P.H.: Chemical composition of atmospheric nanoparticles during nucleation events in Atlanta*, J. Geophys. Res.,* 110, Art. No. D22S03 NOV 8, doi:10.1029/2005JD005912, 2005.

Stein, S.W., Turpin, J.B., Cai, X., Huang, P.F., McMurry, P.H., Measurements of relative humidity dependent bounce and density for atmospheric particles using DMA-impactor technique, *Atmos. Environ.* 28, 1739-1746, 1994.

Slowik, J., Stainken, K., Davidovits, P., Williams, L. R., Jayne, J. T., Kolb, C. E., Worsnop, D. R., Rudich, Y., DeCarlo, P., and Jimenez, J., Particle Morphology and Density Characterization by Combined Mobility and Aerodynamic Diameter Measurements. Part 2: Application to Combustion Generated Soot Particles as a Function of Fuel Equivalence Ratio, *Aerosol Sci. Technol*., 38(12):1206–1222, 2004.

Virtanen, A., Marjamäki, M., Ristimäki, J., Keskinen, J.,. Fine particle losses in electrical low-pressure impactor, *Journal of Aerosol Science*, vol 32, pp 389-401, 2001.

Virtanen, A., Rönkkö, T., Kannosto, J., Ristimäki, J., Mäkelä, J., Keskinen, J., Pakkanen, T., Hillamo, R., Pirjola, L., Hämeri, K., Winter and summer time size distributions and densities of traffic related aerosol particles at a busy highway in Helsinki. *Atmos. Chem. Phys.*, 6, 2411-2421, 2006.

Wagner, R., Möhler, O., Saathoff, H., Schnaiter, M. ja Leisner, T., New cloud chamber experiments on the heterogeneous ice nucleation ability of oxalic acid in the immersion mode. *Atmos. Chem. Phys.*, *11* (5), 2083–2110, 2011.

Wall S., John W., Wang H.-C., Measurements of kinetic energy loss for particles impacting surfaces, *Aerosol Sci. Technol.*, 12, 926-946, 1990.

Yu H., McGraw R., Lee S.-H., Effects of amines on formation of sub-3 nm particles and their subsequent growth. *Geophys. Rev. Lett*. 39, L02807, doi:10.1029/2011GL050099, 2012.

Zobrist, B., Marcolli, C., Pedernera, D. A., and Koop, T.: Do atmospheric aerosols form glasses? *Atmos. Chem. Phys*., 8, 5221-5244, 2008.

Tampereen teknillinen yliopisto
PL 527
33101 Tampere

Tampere University of Technology
P.O.B. 527
FI-33101 Tampere, Finland

ISBN 978-952-15-2902-3
ISSN 1459-2045